UNIVERSITY OF OKLAHOMA
GRADUATE COLLEGE

FRACTURE CHARACTERIZATION OF THE MISSISSIPPI LIME UTILIZING WHOLE CORE, HORIZONTAL BOREHOLE IMAGES, AND 3D SEISMIC DATA FROM A MATURE FIELD IN NOBLE COUNTY OKLAHOMA

A THESIS

SUBMITTED TO THE GRADUATE FACULTY

in partial fulfillment of the requirements for the

Degree of

MASTER OF SCIENCE

By

VERLIN GLENN STEARNS III
Norman, Oklahoma
2015

FRACTURE CHARACTERIZATION OF THE MISSISSIPPI LIME UTILIZING WHOLE CORE, HORIZONTAL BOREHOLE IMAGES, AND 3D SEISMIC DATA FROM A MATURE FIELD IN NOBLE COUNTY OKLAHOMA

A THESIS APPROVED FOR THE
CONOCOPHILLIPS SCHOOL OF GEOLOGY AND GEOPHYSICS

BY

____
Dr. Kurt Marfurt, Chair

____
Dr. Matthew Pranter

____
Dr. Bradley Wallet

Dedication

I would like to dedicate this thesis to my children. It's never too late to learn.

Acknowledgements

This thesis would not have been written without the support of so many people. Kurt Marfurt, Matthew Pranter, Bradley Wallet, Abdulmohsen Alali and Bob Davis provided much needed support, time, and wisdom. I would like to especially thank Bruce Miller with Redfork Energy for providing the data, geological insight, and exploration motivation for this thesis. Software for image and seismic interpretation was provided by AASPI, Schlumberger, and CGG. Lastly, I would like to thank my family for their sacrifice and support during this process.

Table of Contents

List of Figures

Abstract

Originally thought to be a simple resource play, recent development of the Mississippi Limestone in northern Oklahoma and southern Kansas has found it to be highly heterogeneous. Previous work supports the hypothesis that natural fractures play a significant role in Mississippian productivity in explaining sporadic vertical well production from intervals that effectively have little or no permeability. For this reason, characterizing the spatial extent, density, and geometry of natural fractures is fundamental in understanding reservoir producibility. Open natural fractures provide a permeable pathway for fluid entry into a wellbore and, to a limited extent, reservoir storage capacity.

The Mississippian interval located in southern Noble county Oklahoma is composed of a series of stacked cleaning upward clinoforms. I integrate seismic attributes and impedance computed from a modern 11 square mile 3D seismic survey with seven horizontal image logs, core analysis, and vertical well log data to map lithology, geomechanical properties, and natural and induced fractures. This integration shows the brittle upper portion of the stacked clinoforms contains small scale, lithology bound, East-West striking mineralized fractures. Although there is no significant correlation between hydraulically fractured horizontal well production and total fractures counts observed in borehole images ($R^2 = 0$), the density of fractures observed directly relates to the lithology and geomechanical unit that the wellbore transects. Wells landed in brittle, low Gamma Ray intervals exhibited more fractures. All horizontal wells analyzed were hydraulically fractured commingling multiple geomechanical units such that quantification of role that the mineralized fractures on

well productivity was inconclusive. Seismically computed volumetric curvature analysis of this data volume is a good indicator for fractures that have formed through structural mechanism within brittle, fracture prone rock. In addition, Seismic impedance positively correlated with first year total fluid (R^2 = 0.34) and gas (R^2 = 0.68) production with higher production in areas of lower impedance.

Introduction

The Mississippi Limestone in northern Oklahoma and southern Kansas has recently been brought back to the forefront in drilling development due to the advent of industrial scale horizontal drilling, hydraulic fracturing, and favorable oil prices. Discovery of this expansive play occurred in the early 20th century and has been developed with over 12,000 vertical wells. According to the Oklahoma Corporation Commission in 2012, 22 percent of the state's 250,000 BBL/Day comes from the play. The Mississippi Lime is composed of varied heterogenic facies but can be generally characterized as a non-porous expansive shelf limestone. Hydrocarbon accumulation resulted in porous intervals in both structural and stratigraphic traps. Large accumulations in porous intervals were exploited economically with vertical wells. However, accumulations in thinner, less porous intervals were difficult to produce economically. These difficult to produce and find reserves are the target of modern oil exploration utilizing horizontal drilling and hydraulic fracturing.

This study integrates borehole images, core analysis, 3D seismic, vertical well log data, and production data to understand and identify remaining reserves and analyze the spatial distribution and influence of natural fractures on well productivity. The area of study covers the Lone Elm field located in Noble County Oklahoma and is limited in extent to township 20N 1E (Figure 1). As of November of 2015, there have been 19 Mississippi Lime horizontal wells drilled and completed in the township (Figure 2). Of these wells, eight are located within the Lake McMurtry seismic survey. Borehole images were acquired and interpreted on seven of these wells. Whole core from the Double Eagle Tubs 3 and the Gulf Oil Flora 1 wells, adjacent to the seismic survey, were analyzed. Only 44 wireline logs, from over 92 vertical Mississippi Lime producing vertical wells, were found and used in the study.

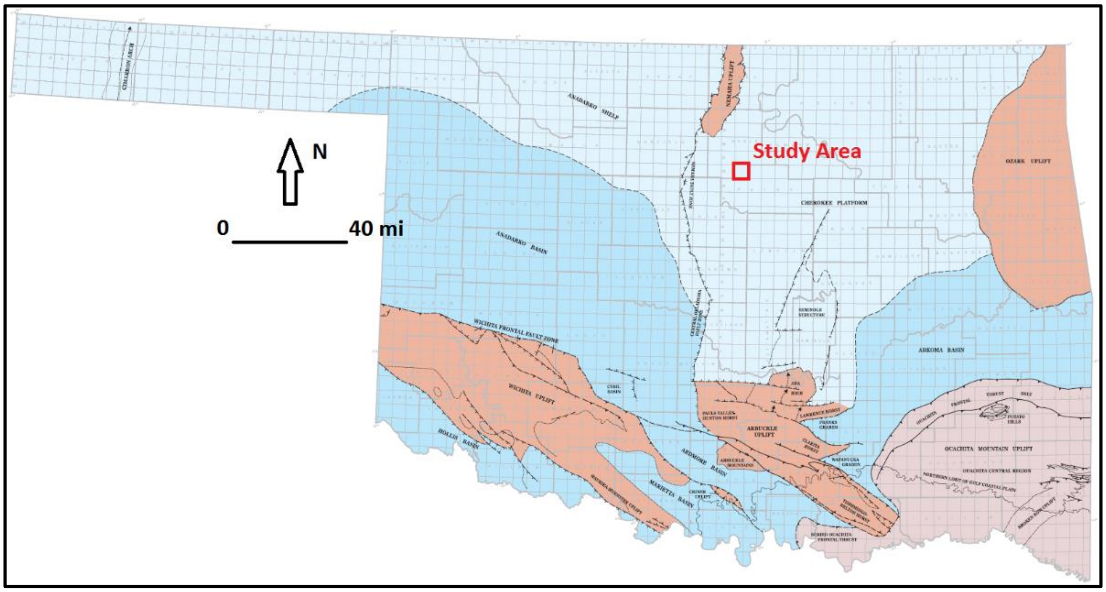

Figure 1. Map of geological provinces of Oklahoma with study area highlighted in red. (Modified from Northcutt and Campbell, 1995)

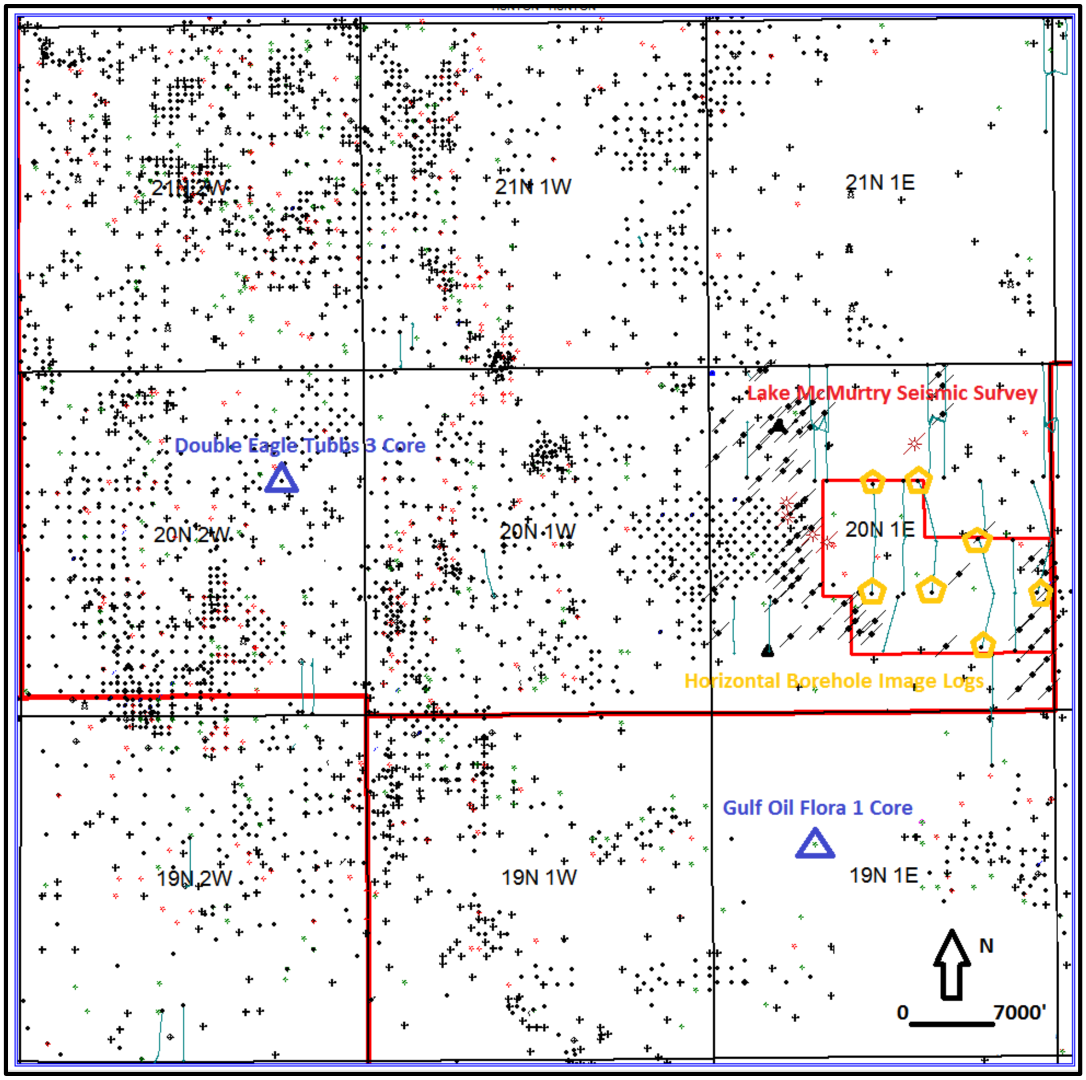

Figure 2. Lake McMurtry 3D seismic survey, within 20N 1E, outlined in red. Orange pentagons indicate horizontal wells with borehole images. Blue triangles highlight the wells with whole core.

Recent research attempting to characterize the Mississippi Lime utilizing a wide range of data has been conducted within proximity to the study area (Figure 3). In separate studies of a 3D survey acquired in Osage Co., OK, Dowdell (2013) and White (2013) were able to identify zones of high porosity and fracture density from 3D seismic attributes and borehole images. Dowdell (2013) found that low impedance from prestack inversion identified areas of thicker tripolitic chert. White (2013) concluded that fractures observed in borehole images were primarily controlled by lithology with possible enhancement from structural curvature. Turnini (2015), working in Kay Co., identified seven lithofacies from core analysis of which four are discernable on open-hole wireline logs. Turnini (2015) determined that tripolitic chert was the main reservoir facies and contributed to higher total fluid production. However, she did not find a one to one correlation with tripolitic chert thickness and oil production and emphasized the need of a trapping mechanism. Trumbo (2014), also working in Kay Co., found a strong correlation between structural lineaments signifying that natural fractures may play a role in productivity. Like Turnini (2015), Trumbo (2014) also found a positive correlation with historical vertical well production and low acoustic impedance, but was disappointed that there was not a solid relationship. Trumbo (2014) admits a major limitation in his dataset is the lack of water production and speculates that high porosities zones may be prolific water producers.

This study continues the investigation of the role of fractures and porosity on horizontal well productivity. Fractures observed in core and borehole images were compared with seismic curvature and well productivity. Furthermore, a post stack seismic inversion was computed and impedance was correlated to horizontal well performance.

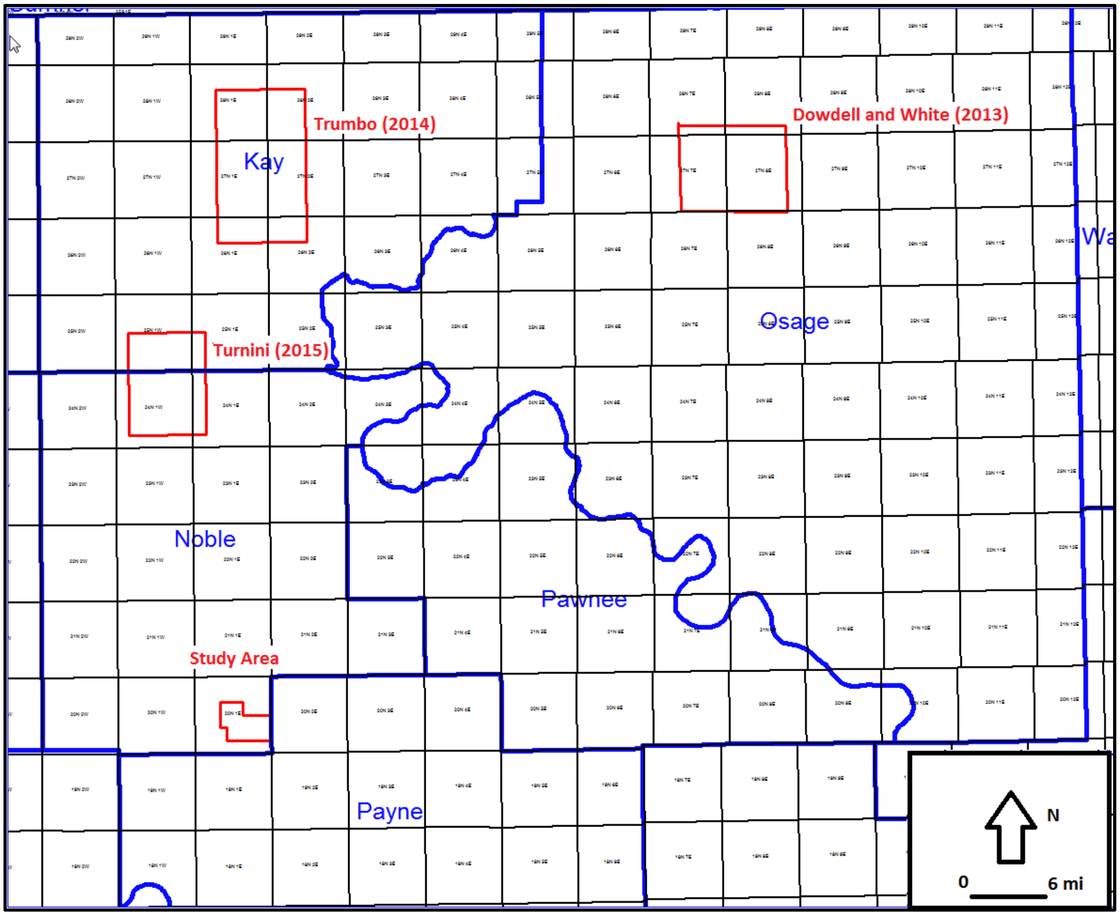

Figure 3. Map highlighting recent and related Mississippian Limestone study outlined in red.

Geologic Setting

The Mississippian Limestone was deposited on a broad continental shelf and is composed of limestone with some chert, shale, and siltstone (Figure 4). The formation is a series of shallowing upward, higher order, progradational wedges that have accumulated within a larger third-order transgressive-regressive cycle (Comer, 1991). Childress and Grammer (2014) found that the higher order wedges compose a complex stacking pattern of facies laterally shifted by Miliankovitch-scale sea level changes (Figure 5). The Mississippian Limestone interval is subdivided into four ages Kinderhookian, Osagean, Meramecian, and Chesterian of which only the Osagean series is present in the study area (Figure 6). During the Kinderhookian, mid-continent seas transitioned from poor to well-oxygenated resulting in shale and limestone deposition on top of organic rich Woodford (Northcutt et al., 2001). The unit is difficult to discern from electrical logs and is often grouped with Woodford or Osagean (Jordan and Rowland, 1959). The Kinderhookian varies in thickness up to over 200 feet in the Northwest, but in central and south Oklahoma, was extensively eroded (Northcutt et al., 2001). Warm, aerated Osagean seas covered Oklahoma while diverse marine fauna prevailed. Osagean rock is composed between 10-30 percent chert which forms from carbonate replacement of silica (Northcutt et al., 2001). The Oseagean varies in thickness upwards to over 500 feet in Oklahoma but averages just over 200 feet within the study area.

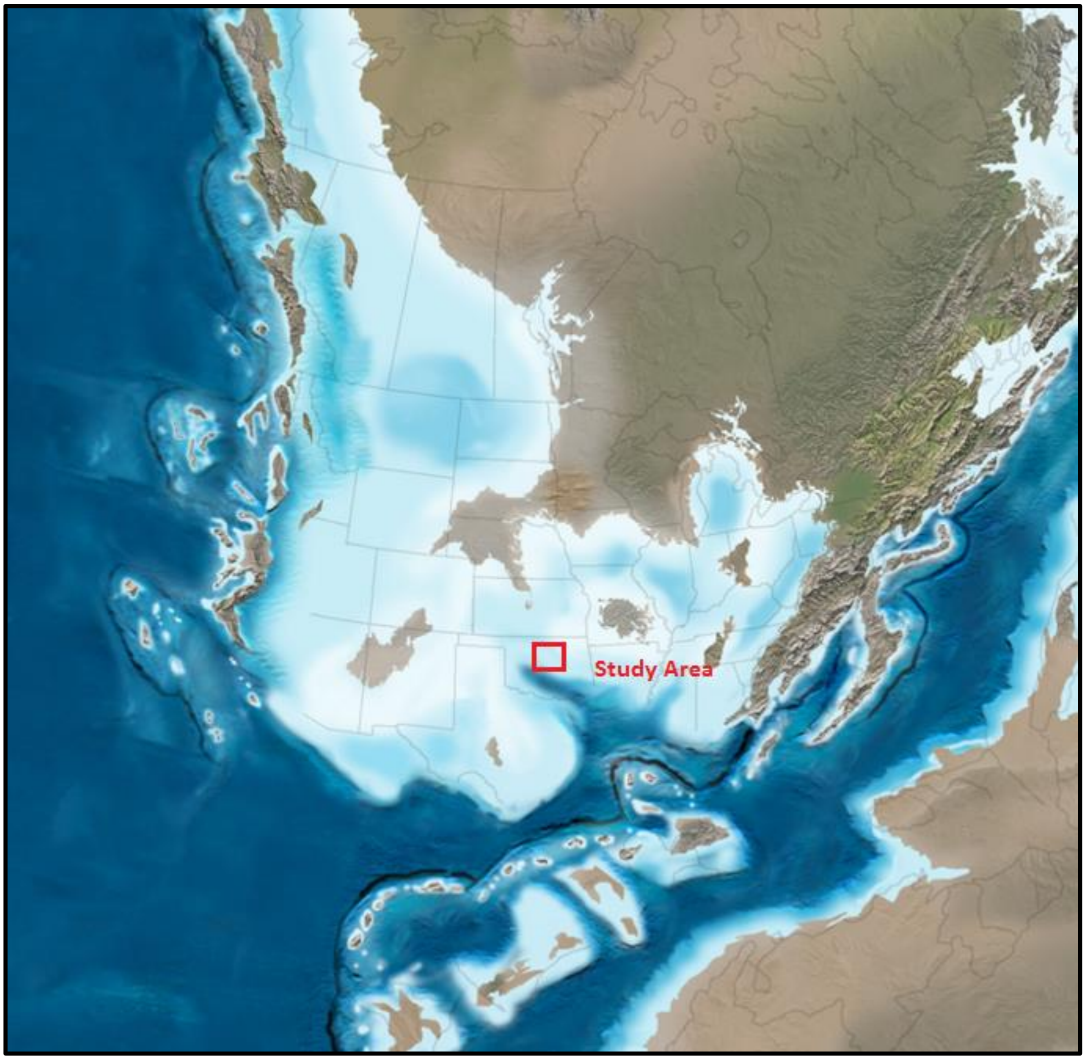

Figure 4. Paleogeographic map during Mississippian with study area highlighted in red illustrating broad continental shelf. (Modified from Blakey, 2015)

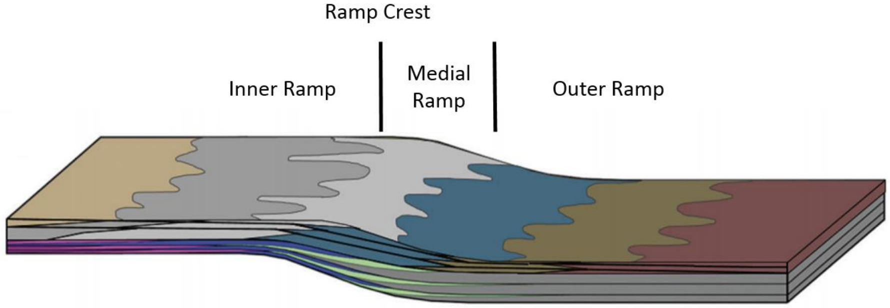

Figure 5. Model illustrates complex stacking of progradational wedges and laterally shifted facies resulting from higher order transgressive-regressive cycles from Milankovitch-scale sea level changes. (Modified from Harris et al., 2011)

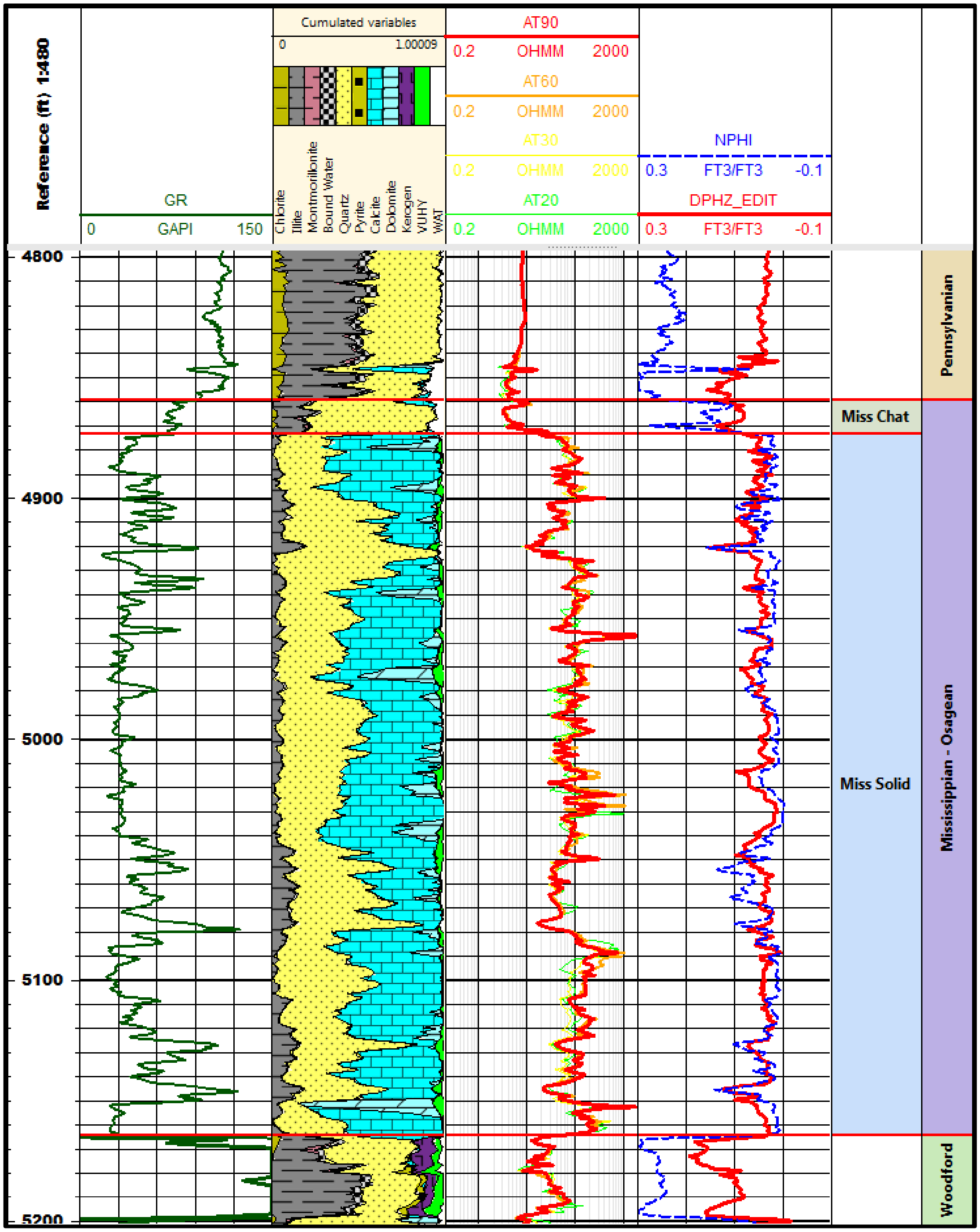

Figure 6. Type log within study area illustrating stratigraphic column. Non calibrated petrophysical interpretation utilizing elemental capture spectroscopy, density porosity, gamma ray, resistivity, and neutron porosity shows varying composition of silicate and calcite within Mississippian interval.

The study area lies approximately 20 miles east of Nemaha uplift (Figure 7). The fault complex is described by Gay (2003) as compressional thrust fault zone with considerable left-lateral strike-slip displacement. The Nemaha uplift had significant growth during the end of the Mississippian during the Ouachita orogeny resulting in erosion and some detrital limestone deposition of the Mississippian Limestone (Dolton and Finn 1989). Meramecian and Chesterian deposits are absent in the study area as they were eroded away (Figure 8).

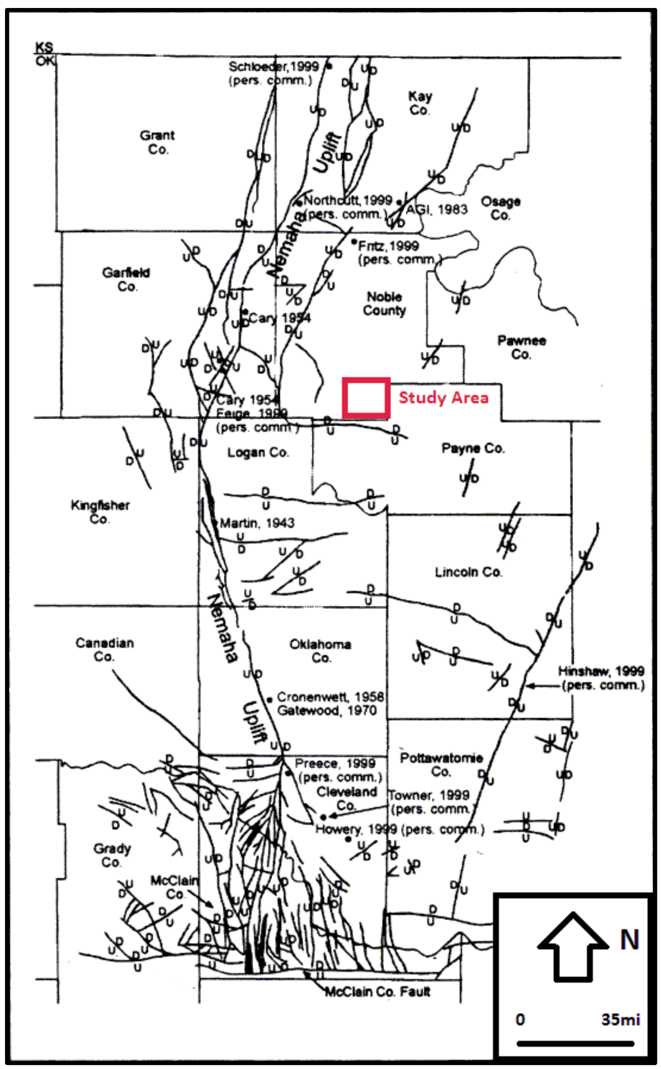

Figure 7. Faults of the Nemaha uplift with study area highlighted in red. (Modified from proprietary map courtesy of Lloyd Gatewood, 1983)

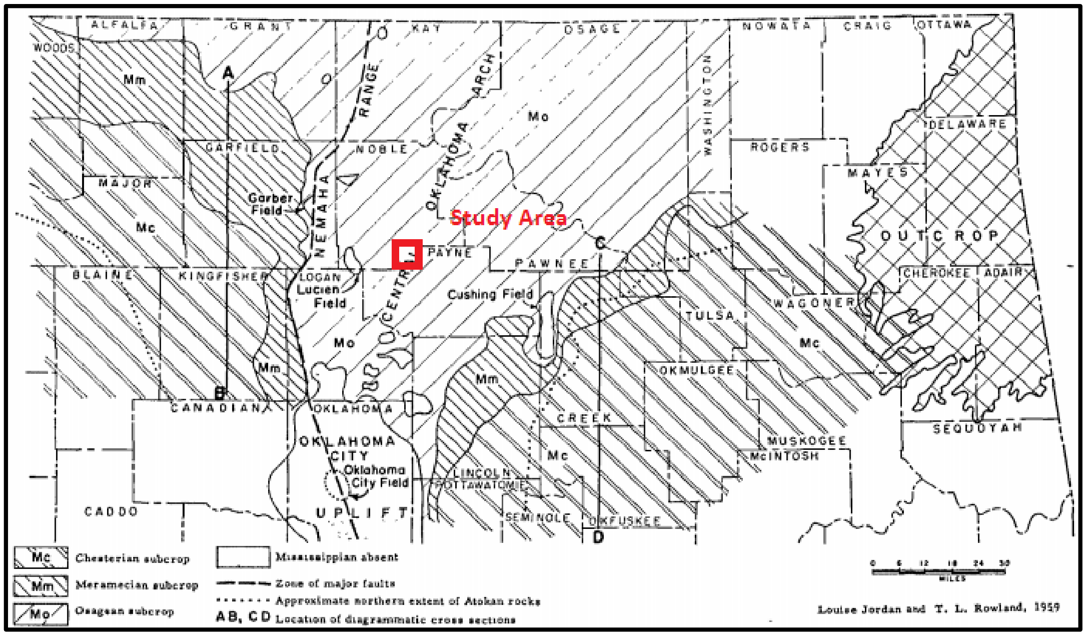

Figure 8. Mississippian subcrop map showing distribution of Oseagean, Meramecian, and Cherterian units in Northern Oklahoma. Study area highlighted in red. (Modified from Jordan and Rowland, 1959)

A thin veneer of detrital or weathered Mississippian deposits, historically referred to as “chat”, covers the Osagean within the study area. Thickness ranges from 5-25 feet (Figure 9). Porosity varies from 5-25 percent within the weathered interval and is generally greater in thicker intervals. Historic vertical well productions in the area shows contribution from both the Osagean and “chat” intervals. Rogers (2001) presented a model for chat development in two different settings (Figure 10). In the first setting, subaqueous erosion of paleo-highs were reworked and deposited in lows. In the second setting, subaerial weathering and dissolution of paleo-highs occurred in-place. Calcite replacement with silica and remnant calcite dissolution occurred in subsequent diagenetic stages. Rogers (2001) concludes that hydrocarbon accumulation in chat reservoirs can occur in both structural and diagenetically controlled stratigraphic traps.

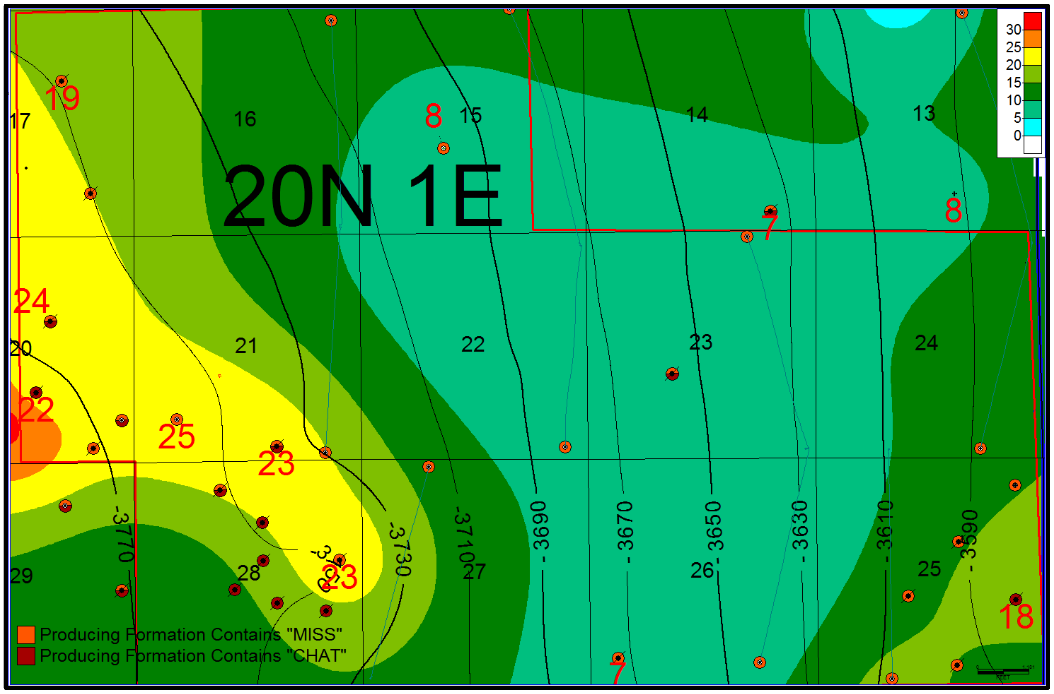

Figure 9. Black contours illustrate the structure of the Mississippian dips toward the west. Colored isopach highlights thickness of the weathered or chat interval. The red numbers represent the observed chat thickness in the vertical well logs that were available. Orange (Osagean) and brown (Chat) well attribute (circle around well) signifies well production from the respective interval.

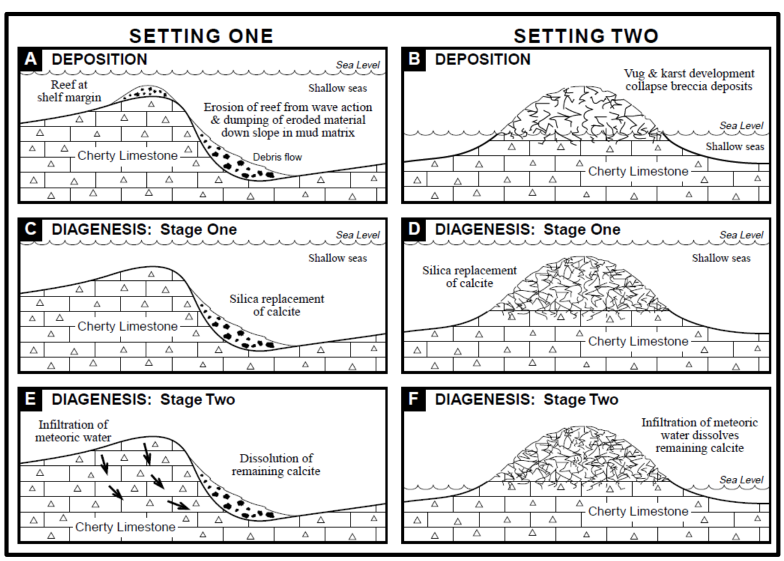

Figure 10. Mississippian chat model illustrating detrital reworking and in situ weathering settings of chat development. Subsequent silica replacement and calcite dissolution further altered sediment into its present form. (Rogers, 2001).

Fractures have been thought to play a significant role in Mississippian productivity in explanation of sporadic vertical well production from Oseagean rock that effectively have no or little matrix porosity (Mazzullo et al., 2011; Trumbo, 2014). Mazzullo (2011) also observed in outcrop a relationship between fractures and brittleness (Figure 11). Zones that had competent limestone and chert were observed to be prone to fracturing while shaly, ductile intervals were not. This configuration of vertical compartmentalization could stratigraphically trap hydrocarbons (Stearns and Friedman, 1972).

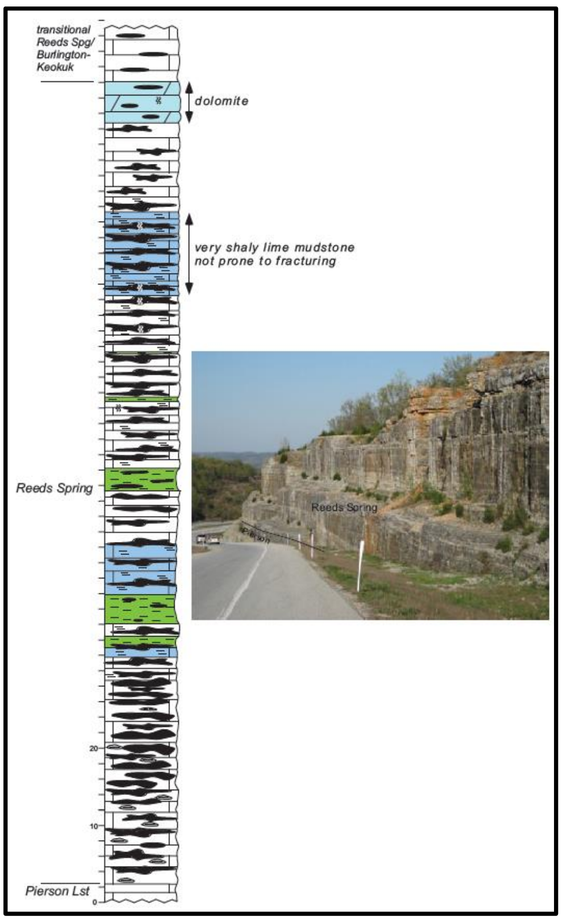

Figure 11. Mazzullo (2011) Reed Spring Formation interpretation of the "Branson North" outcrop in Stone County, Missouri. Shale intervals are highlighted in green. Shaly limestones are in blue. These intervals are interpreted to be vertical permeability barriers and lack natural fractures.

A major goal of seismic evaluation of resource plays is to identify natural fractures. Large fractures and faults are often easily identified in amplitude and coherence volumes. Smaller fractures, however, are below seismic resolution and are difficult to directly measure. Structural curvature, the measure of the curvature of a surface, is thought to correlate with fractures (Figure 12). Strata with high curvature that have been folded from tectonic stress have by definition been strained. Seismic curvature has been used as a proxy to identify highly strained zones likely to be fractured (Hart, 2002; Sigismondi, 2003; Chopra and Marfurt, 2010; Staples 2011; White 2013). Staples (2011), White (2013), and Cahoj (2014) found excellent, but non-linear, correlation between curvature and fracture intensity in clay modeling experiments. They also found positive relationships between seismic curvature and fractures identified in borehole images.

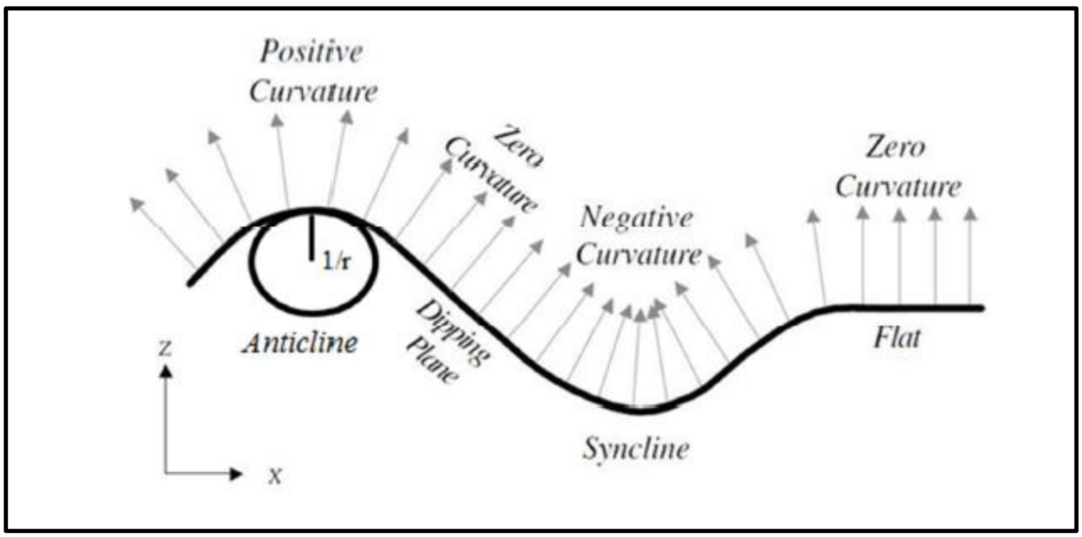

Figure 12. The curvature of a surface is computed from the equation k=1/r, where r is the radius of curvature of a circle that best fits the surface. (Roberts, 2001)

While tectonic folding is perhaps the most common cause of fracture generation, other processes exist. Nelson (2001) expanded on the Stearns and Friedman (1972) fracture classification model by differentiating fractures from tectonic and non-tectonic origins. Tectonic fractures were further categorized into either structural related or regional; while non-tectonic fractures were classified as either contractional or surface related. Contractional fractures result from the change in the bulk volume of the rock which can occur from desiccation, thermal gradients, syneresis, and mineral phase changes (Nelson, 2001). Such shrinkage fractures, due to diagenetic de-watering of chert, have been identified in Oseagean outcrop by Manger (2014). Surface related fractures are created when overburden is removed during weathering. Young (2010) observed three episodes of fracturing Mississippian related to uplift, burial, and hydrothermal origins in analysis of thin sections from core (Figure 13). Understanding the mechanism of fracturing is crucial in understanding their spatial distribution especially in rock that has undergone multiple modes of fracturing.

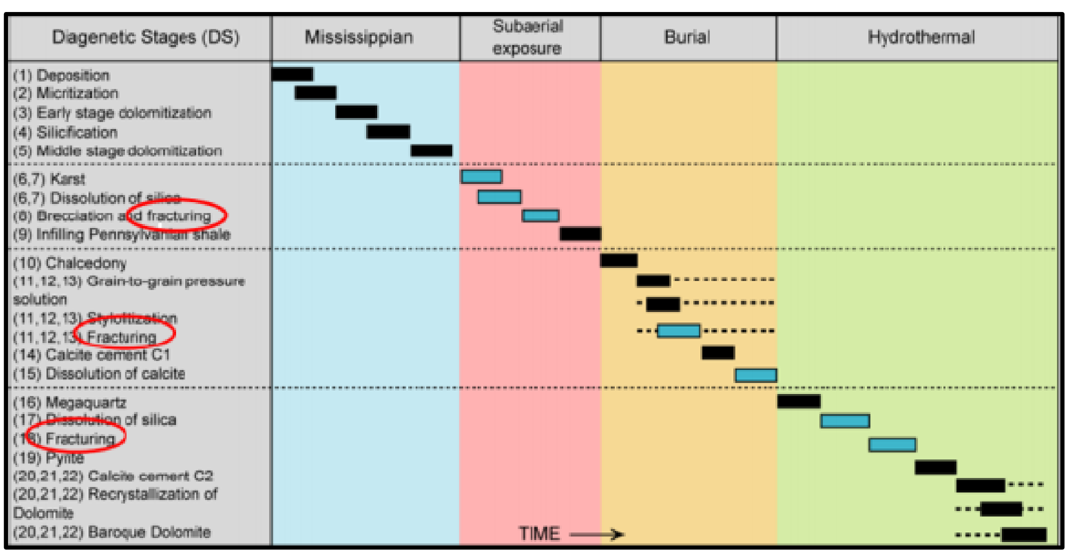

Figure 13. Mississippian paragenetic sequence with three episodes of diagenetic fracturing circled in red (modified from Young, 2010).

This study continues the investigation of the role that fractures and porosity play in Mississippian Lime horizontal well productivity. The data includes modern 3D seismic, limited vertical well log data, seven borehole images acquired in horizontal wells, two cores from vertical wells, and production data. I begin with direct fracture interpretation of the horizontal image logs that are located within the seismic survey. Then, I evaluate core from two nearby vertical wells outside the survey. With this insight, I am able to correlate fractures to volumetric curvature and impedance computed from the seismic data. I conclude with a correlation of first year production to the well log and seismic measurements (Figure 14).

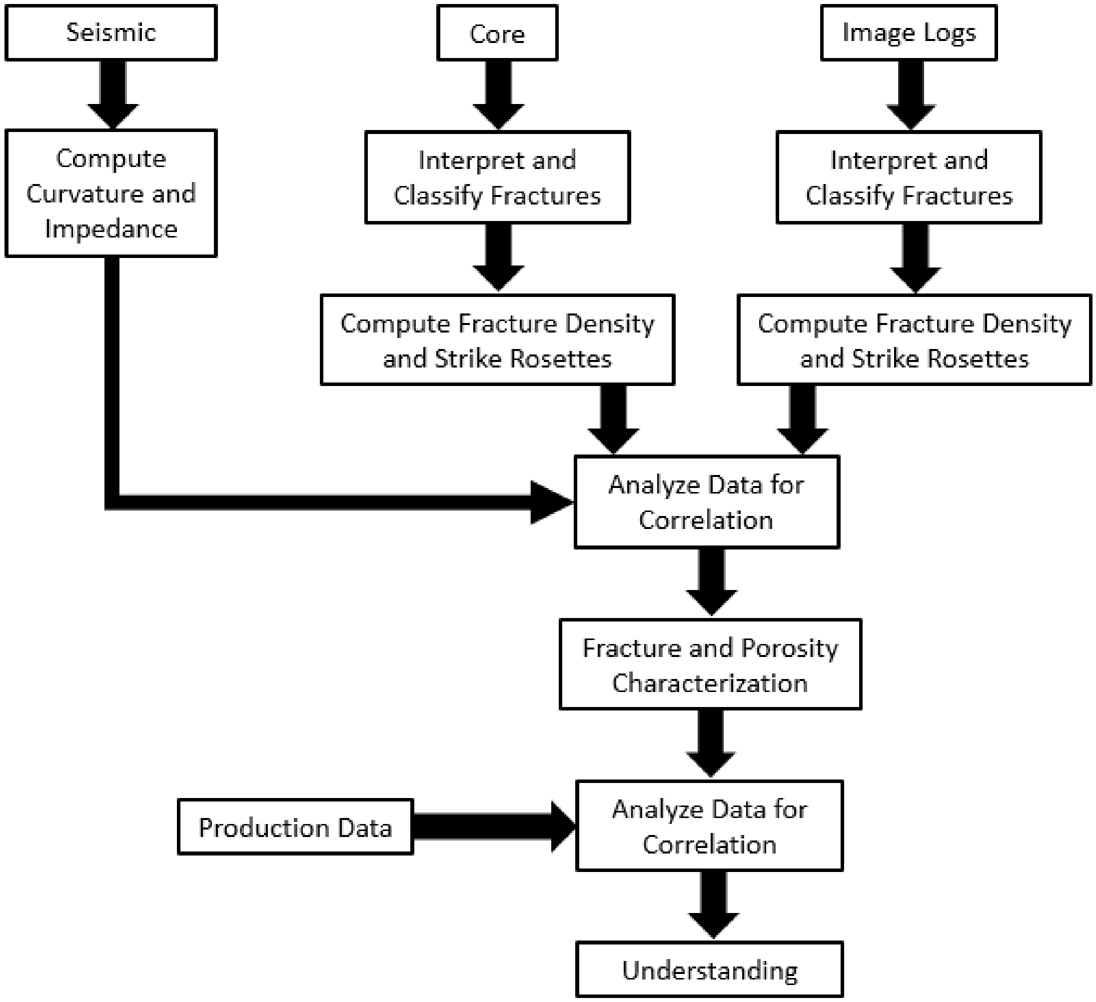

Figure 14. Generalized workflow used in this study begins with seismic attribute computation and fracture interpretation of core and image logs. This data is analyzed for correlation and used to characterize fracture and porosity distribution. The characterization is further correlated to production data to understand influence on well productivity.

Borehole Image Interpretation

Fractures were identified and classified as either resistive or conductive based on the relative resistivity difference of the fracture compared with the matrix. Resistive fractures are interpreted to be mineralized, and therefore impermeable to conductive mud invasion into the plane of the fracture. Mineralized fractures often have a distinct "halo" effect on the image log due to an artifact of data acquisition. Conductive fractures are interpreted to be open to conductive mud invasion. One of the biggest challenges in interpreting fractures in horizontal Mississippian wells is differentiating between drilling induced and natural fractures. In the study area, the natural fracture orientation is the same direction as current day maximum horizontal stress. Using strike orientation to differentiate between the fractures is not possible as they both strike in the same orientation. Another method for differentiating drilling induced from natural fractures in a horizontal well is by observing the location of the fracture in the wellbore. Induced fractures often form on the top and bottom of the wellbore as the rock is more prone to failure where it is in tension. This method is not applicable in the Mississippian because of the interbedded nature of the rock. Lithology bound natural fractures also appear on the top and bottom if the well is cutting down or up into a bed that contains fractures. In this situation, it is impossible to differentiate the two. For this reason, no attempt was made to differentiate between drilling induced from natural fractures within the conductive fracture set. Strike rosettes were created from fracture orientation separated by well and fracture classification. A compilation of the results along with examples of conductive and resistive fractures can be found in Appendices A and C.

Core Analysis

Two vertical cores from near the study area were analyzed for the presence and nature of natural fractures. The first core examined was from the Gulf Oil Flora 1, acquired in 1954, approximately 3 miles south of the study area. The 1.5-inch whole core was taken from the top of the Mississippian interval (4680-4696 ft). The two distinctive lithologies observed were massive lime mudstone and bedded chert. There was no presence of tripolitic chert or “chat”. A vertical line drawn along the core is thought to mark the segmented core’s relative orientation with respect to each other. Fractures were counted and classified as either possibly open or mineralized. The open fractures are described as “possible” because of the difficulty in distinguishing between an open natural fracture and one that was induced after core retrieval. The orientation of the fractures was approximated in reference to the black orientation line. Pictures of the whole core can be found in Appendix B. Fracture densities and strike rosettes were created from the data and compiled with well log data (Figure 15).

The second core examined was from the Double Eagle Tubbs No. 3 acquired in 1981 approximately 10 miles west of the study area. The three-inch core was slabbed and covers more than half of the upper portion of the Mississippian interval (5058-5141.5 ft). The three distinct lithologies observed were wavy bedded lime mudstone, planar bedded lime mudstone, and bioturbated lime mudstone. Fractures were counted and classified as either possibly open or mineralized. Approximating fracture orientation was not possible because the core was slabbed. Fracture densities were calculated and compiled with well log data (Figure 16). The core data were depth shifted ten feet up based on correlation of Gamma Ray and interpreted lithology. This shift is reasonable considering the nine feet in depth discrepancy between driller (5300 ft) and logger (5291 ft) total depth.

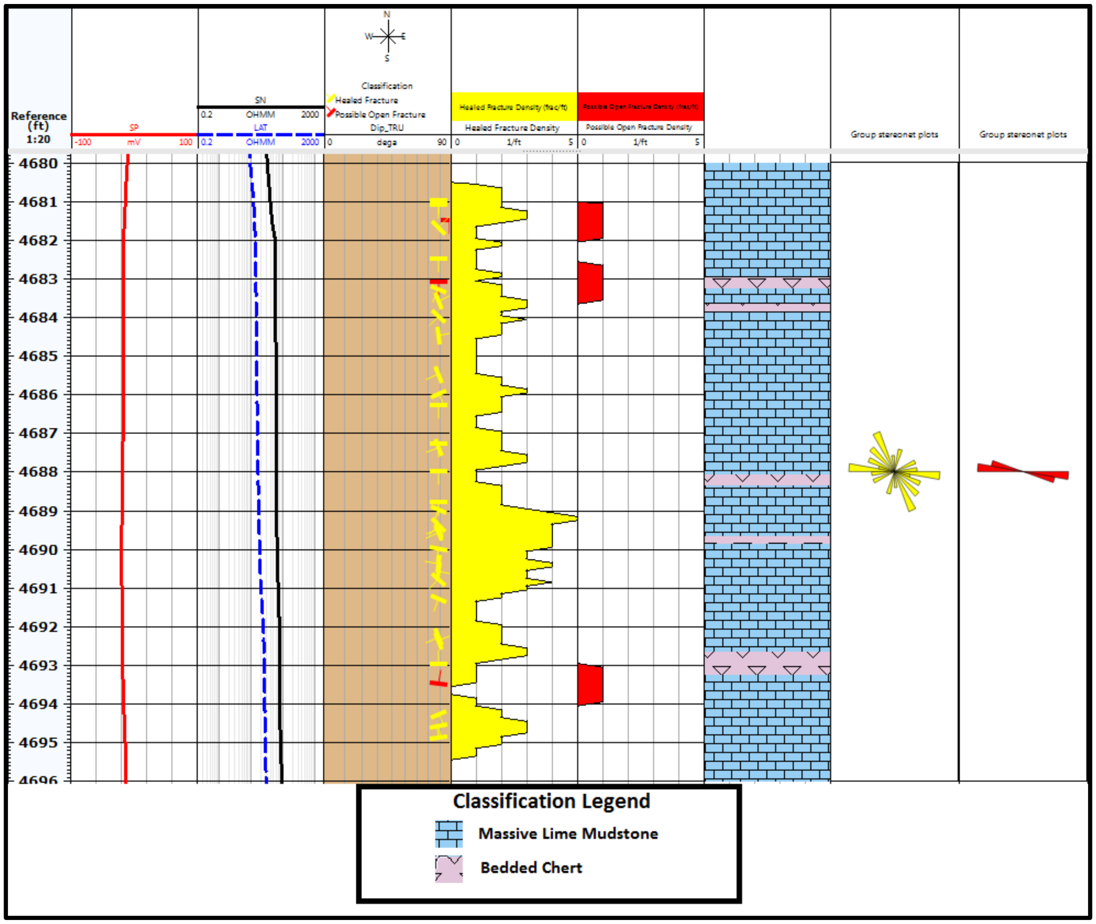

Figure 15. Core interpretation from the Gulf Oil Flora 1. SP is plotted in track one from -100 mv to 100 mv. Short Normal and Laterolog are plotted in track two from 0.2 to 2000 ohmm. Fracture orientation and depth location are located in track three. Yellow fractures are mineralized. Red fractures are classified as possibly open. The dip angle was not measured. Track four contains mineralized fracture density in fractures per foot scaled zero to five. Track five contains possibly open fracture density in fractures per foot scaled from zero to five. Track six contains the facies interpretation with the classification legend below the log. Tracks seven and eight contain strike rosettes of the mineralized and possibly open fractures.

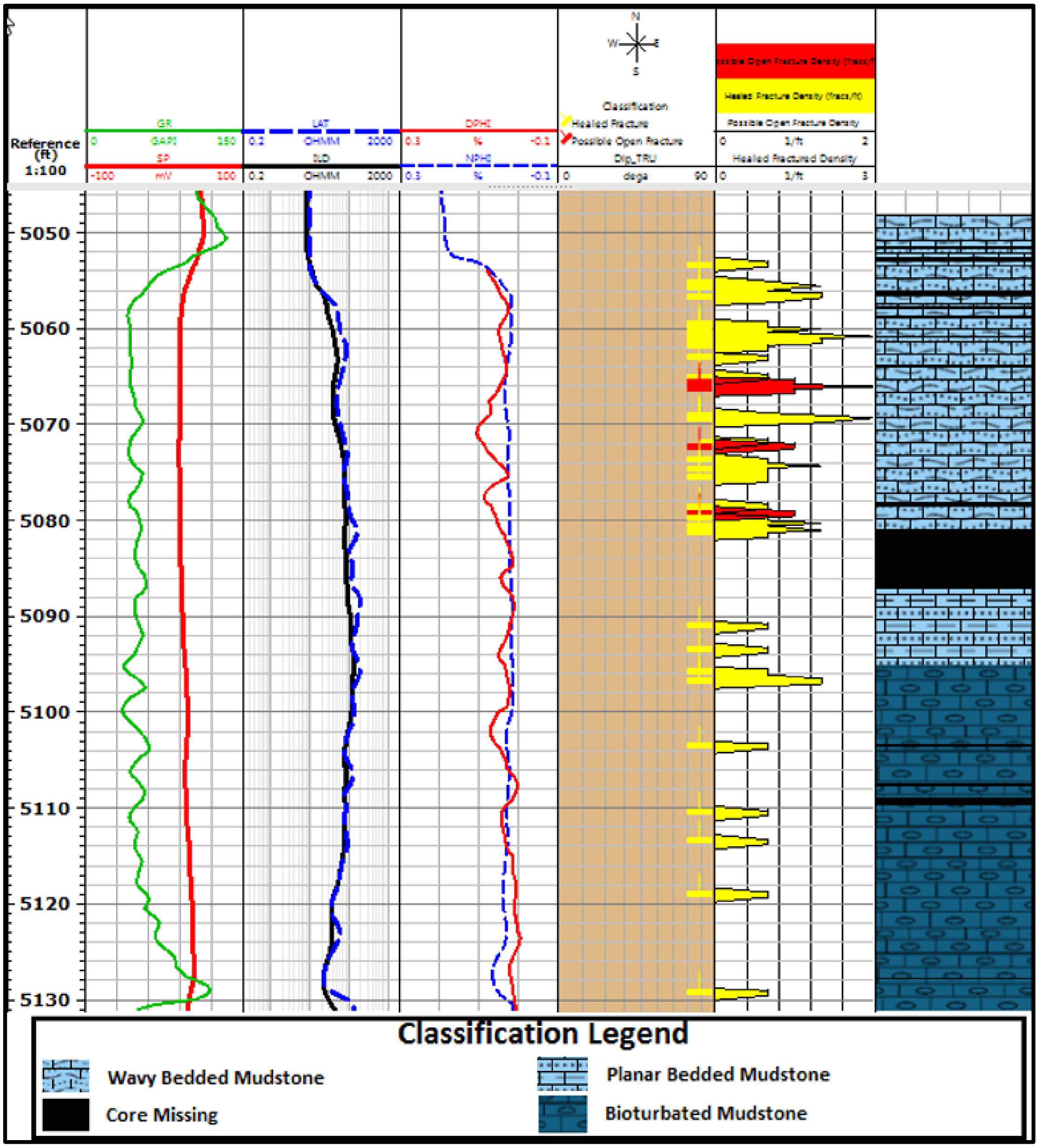

Figure 16. Core interpretation from the Double Eagle Tubbs No. 3. SP is plotted in track one from -100 mv to 100 mv along with Gamma Ray from 0 to 150 GAPI. Short Normal and Induction are plotted in track two from 0.2 to 2000 ohmm. Density and Neutron porosity are plotted in track three from 30% to -10%. Fracture orientation and depth location are located in track four. Yellow fractures are mineralized. Red fractures are classified as possibly open. The dip angle of the fractures was not measured. Track five contains mineralized fracture density (yellow) in fractures per foot scaled zero to five. Possibly open fracture density is plotted in red. Track six contains the facies interpretation with the classification legend below the log. Most fractures were observed to be in low Gamma Ray rock.

Core and Image Log Fracture Reconciliation

The number of mineralized fractures in both observed cores were quite numerous. Height and relative size of the fractures appear small. Due to limits in core size, quantifying the exact height and length of fractures is not possible in most cases. However, most of the fractures had observable height termination within the core. This leads me to believe that the height and length of the fractures are on an order of magnitude of inches and feet. Most of the fractures observed in the core were mineralized with certainty. This contradicts the high number of conductive fractures observed in the borehole images. There were numerous fractures observed in the images that appeared partially resistive and conductive as though there was slight fluid invasion into the fracture plane (Figure A5 and A6).

Some of the fractures that appear conductive on the image logs could indeed be partially mineralized. Complete mineralization would be required to block all fluid entry into the fracture plane. There is some evidence from the whole core data that suggest partial mineralization (Figure B6 A). Fluid entry into the fracture plane could be enhanced by reactivation of the fracture from drilling and fluid stresses. In essence, the mineralized fracture could provide an inherent weakness for the propagation of an induced fracture. Another possible explanation is that the small scale mineralized fractures may be below the resolution of the borehole imager. Also, the conductive fractures observed in the borehole images could possibly all be drilling induced. However, one cannot ignore the positive correlation in fracture orientation between the mineralized fractures in the Gulf Oil Flora 1 (Figure 15) and the conductive fractures observed in the horizontal wells in sections 15 and 16 in 20N 1E (Figure A7). The arbitrary black reference line on the Gulf Oil Flora 1 well may have purposely marked the north orientation of the core. No offset was applied to the orientation of the fractures. The bimodal distribution of the fracture sets (East-West and Northeast-Southwest) from the two datasets match exceptionally well.

Another positive correlation of the data is the relation of fractures and lithology. Fracture density in the Double Eagle Tubbs No. 3 correlated well with Gamma Ray and lithology. More fractures were observed in cleaner, more brittle rock in comparison with the ductile shaly lime mudstone. Gamma Ray and conductive fracture density from the image logs show the same relationship as can be seen in Appendix C. Figure C1 shows the correlation of the Gamma Ray markers in the vertical wells located within the seismic survey. The Gamma Ray markers appear to mark transgressive-regressive cycles along clinoform dip (Figure C2). The fracture density observed in the horizontal wells directly relates to the wellbore's location in the section. Fracture density is high when the wellbore is in the more brittle, lower Gamma Ray, portion of the clinoform (Figure C3-8). As the wellbore transects the higher Gamma Ray, more ductile, portion of the clinoform, fracture density decreases (Figure C3-8).

Image Fracture Density Comparison with Volumetric Curvature

Fracture density from image log data was computed and smoothed over 100 feet to better match seismic resolution. Most-positive curvature, most-negative curvature, and shape index were calculated using AASPI software. In the following compilation (Figure 16), fracture data is displayed as a 3D pipe along the wellbores with red indicating more than five and blue indicating zero fractures per foot. Gamma Ray is displayed as a 2D log along the wellbores with yellow indicating 10 GAPI or less and brown indicating 80 or more. Most-positive and most-negative curvature is co-rendered with seismic amplitude in black and white. For reference, a depth structure map of the top of the Mississippi Lime and corresponding horizon slices through shape index, most-positive curvature, and most-negative curvature are presented in Appendix D.

In Figure 17, yellow circles indicate areas of low Gamma Ray that are highly fractured. Brown circles indicate areas that have high Gamma Ray and no fractures. As discussed previously, the natural fractures appear to be contained within the cleaner more brittle rock. In comparison with curvature, green arrows indicate areas of good correlation with curvature. White arrows indicate areas where there is strong curvature with little or no fractures observed. Black arrows indicate areas with a significant number of fractures, low Gamma Ray, but no curvature anomaly, indicating curvature alone cannot serve as a fracture proxy. A cross-plot of curvedness versus fracture density is displayed in Figure 18.

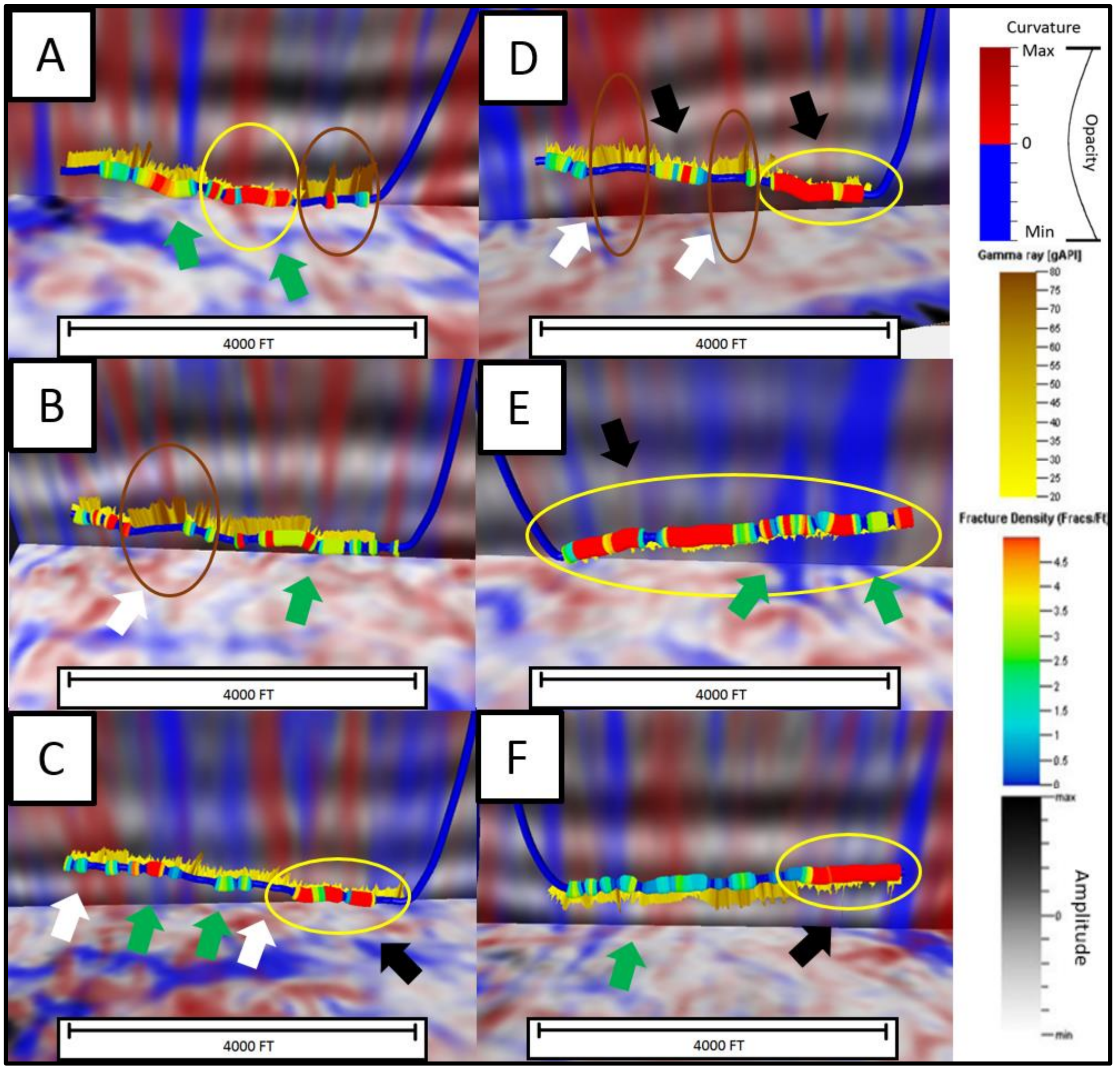

Figure 17. Fracture data displayed as a 3D pipe along the wellbores with red indicating more than five and blue indicating zero fractures per foot. Gamma Ray is displayed as a 2D log along the wellbores with yellow indicating 10 GAPI or less and brown indicating 80 or more. Most-positive and most-negative curvature is co-rendered with seismic amplitude in black and white along with fracture data. Green arrows indicate areas of good correlation with curvature. White arrows indicate areas where there is strong curvature with little or no fractures observed. Black arrows indicate areas with lots of fractures, low Gamma Ray, and no curvature anomaly.

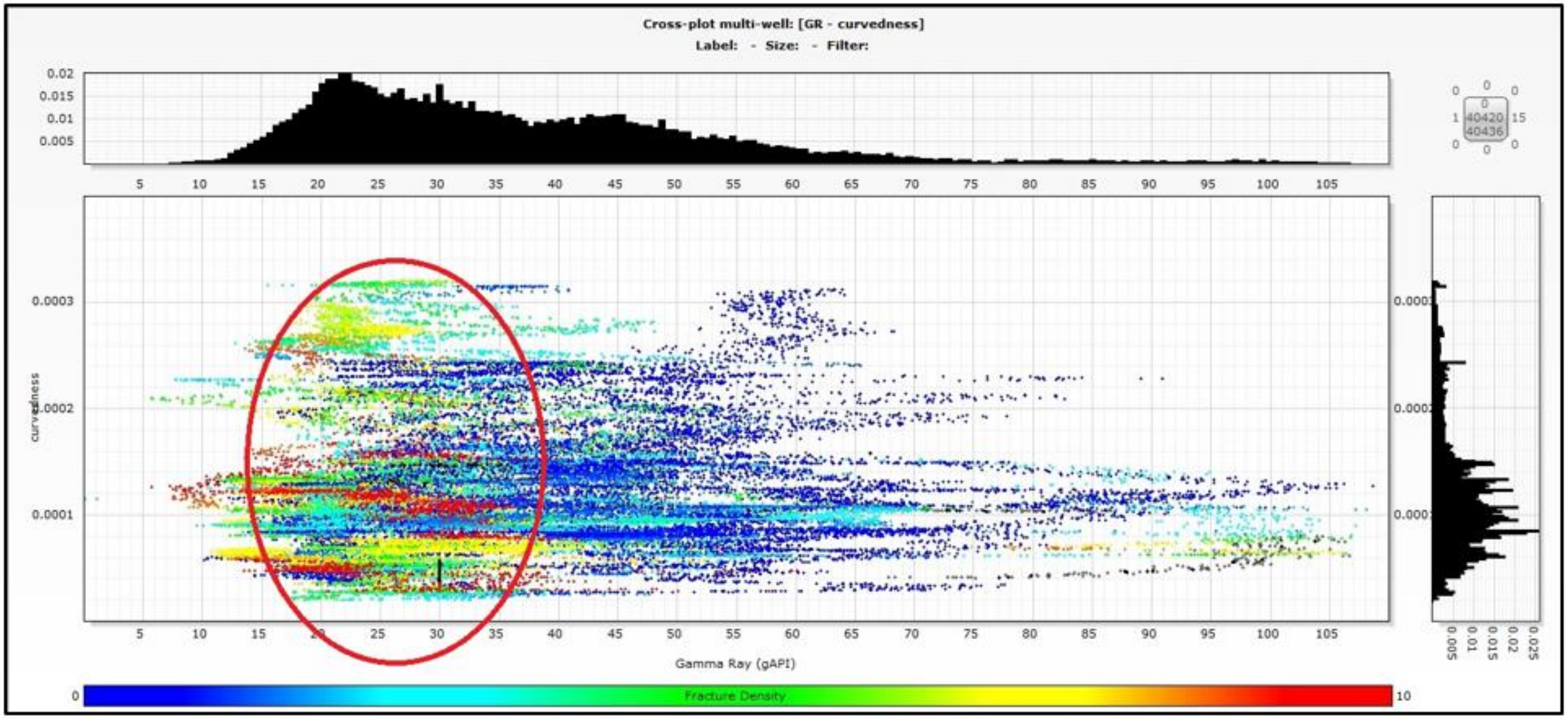

Figure 18. Curvedness (root mean square of the most-positive and most-negative curvature) versus Gamma Ray shown above with points colored based on fracture density. Most of the fractures are observed to be in low Gamma Ray rock (red circle). Fracture density appears to be driven more by lithology than by curvedness.

Image Log Fracture and Seismic Curvature Reconciliation

I evaluate three hypotheses to explain the poor correlation between structural curvature and fractures observed in the image log data. First, volumetric curvature indicates present day rather than paleo structural deformation. The structure may have been deformed and fractured in the past and then “un-deformed”. Such up and down movement of strike-slip blocks have been documented in Mississippi Lime surveys in neighboring Osage Co., OK (Rector, 2011). Second, the fractures were not formed from structural folding, but rather are due to uplift, erosion, and diagenesis during the late Mississippian Ouachita orogeny. The fractures that we observe today could be caused by contractional or surface related mechanisms as described by Norman (2001) and observed in Mississippian core by Young (2012) and outcrop by Manger (2014). Third, the conductive fractures observed in the borehole images are drilling induced. However, since the wells were drilled with water, it is unlikely that the fractures were hydraulically induced. However, the cleaner brittle rock could have mechanically fractured during the drilling process. Drilling induced fractures are often observed in vertical wells and provide a diagnostic orientation of maximum horizontal stress. Controverting this explanation is the observation of mineralized fractures in the Double Eagle Tubbs No. 3 and the Gulf Oil Flora 1 cores and in outcrop by Mazzullo (2011). Although this is the least likely explanation, I am convinced that at least some of the included conductive fractures are drilling induced. As discussed previously, distinguishing induced from natural using conventional interpretation methods was not possible.

Image Log Fractures and Well Production Analysis

Figures 19 and 20 show total fracture counts interpreted from the image logs cross plotted with total fluid and gas production. Total fluid production was used instead of just oil because the wells produce approximately 85 percent water. Both cross plots show that fractures observed in borehole images have very little, if any, correlation with well productivity. However, as previously discussed, fracture density observed is dominated by the lithology in which the wellbore is landed. Wellbores that were landed in brittle rock have more transecting fractures. Likewise, wellbores that traversed and stayed in ductile zones encountered few fractures. At first look, the data suggests that fractures play no part in fluid storage capacity and reservoir permeability. However, consideration must be given to the fact that the reservoir consists of several vertically stacked mechanical units. The fractures characteristics that are observed in borehole images are only valid for the mechanical unit that the wellbore is in. To further complicate the analysis, all the wells were hydraulically stimulated. Wells that have less transecting natural fractures are likely well connected to the natural fracture system after stimulation.

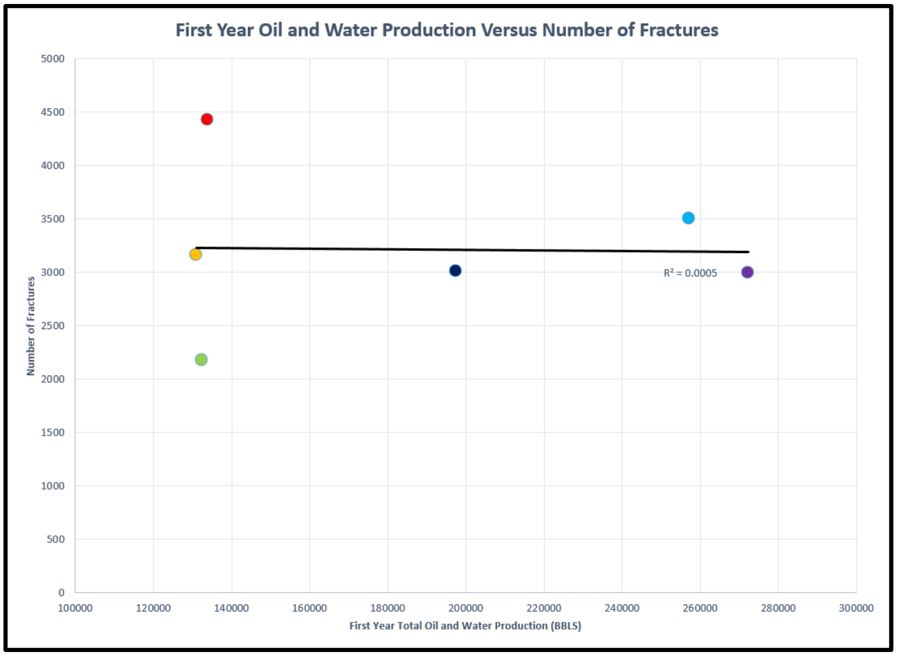

Figure 19. Cross plot of first year total fluid production (oil and water) versus number of fractures observed in borehole images shows no correlation ($R^2 = 0$). Total fluid includes both oil and water production. Points are colored by well and are the same in all figures.

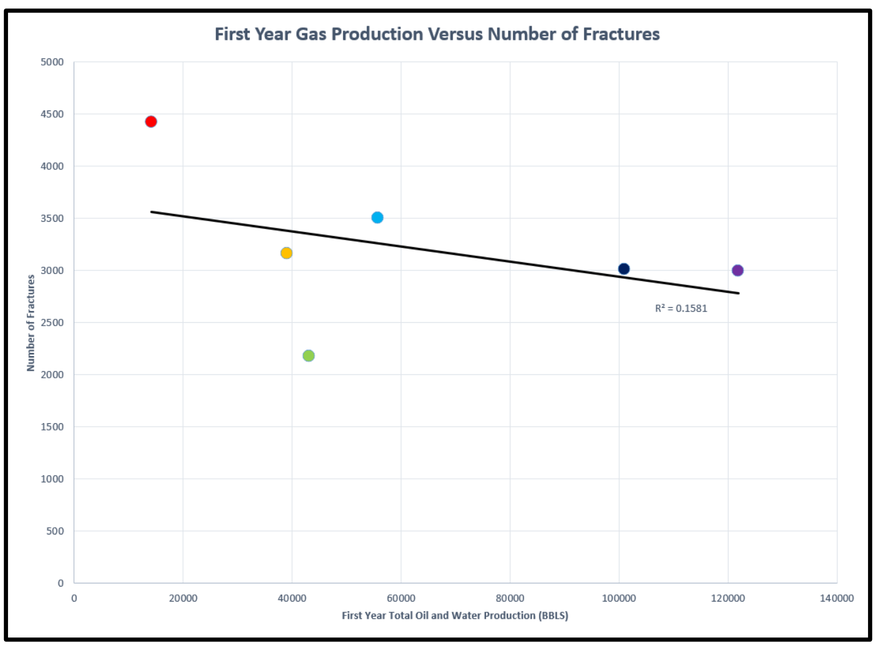

Figure 20. Cross plot of first year gas production versus number of fractures observed in borehole images shows no correlation ($R^2 = 0.16$). Points are colored by well and are the same in all figures.

Another point to consider is that most fractures observed in core were mineralized. Completely mineralized fractures could be a hindrance to reservoir productivity if they were to act as permeability barriers. Conversely, mineralized fractures may improve the complexity and surface area of hydraulically fracture network if the fractures become reactivated during stimulation. Evidence of mineralized fracture reactivation was observed in the acquired images (Figures A5 and A6).

Seismic Impedance and Well Production Analysis

Seismic impedance was computed from density and sonic velocity data using commercial software. Seismic impedance was averaged throughout the entire Mississippian interval and compared with horizontal well production (Figures 21 and 22). The impedance data shows a fair correlation compared with "chat" thickness considering the isopach (Figure 9) is limited in well control with only 10 data points and does not account for variability in porosity. Small errors in the interpreted top of Mississippian "chat" from the seismic volume is likely because of the small contrast in impedance with the overlying Pennsylvanian shale. Of the 23 vertical wells completed in the Mississippian 16 were completed in the "solid" and 12 were completed in the "chat". Both intervals were productive and should be combined in acoustic impedance and production analysis considering likely coupled hydraulic fracture stimulation.

Acoustic impedance was also averaged within the hydraulic fracture stimulated volume (assuming a 1500 feet hydraulic fracture half-length) for each well and cross plotted versus first year production (Figures 23 and 24). A fair correlation ($R^2 = 0.34$; P value = 0.252) was found between first year total fluid production (oil and gas) and acoustic impedance. A better correlation ($R^2 = 0.68$; P value = 0.0447) was found with first year gas production. The mature field has been depleted from 23 vertical wells. Reservoir pressure could possibly be below bubble point resulting in presence of scattered free gas within the poor volume.

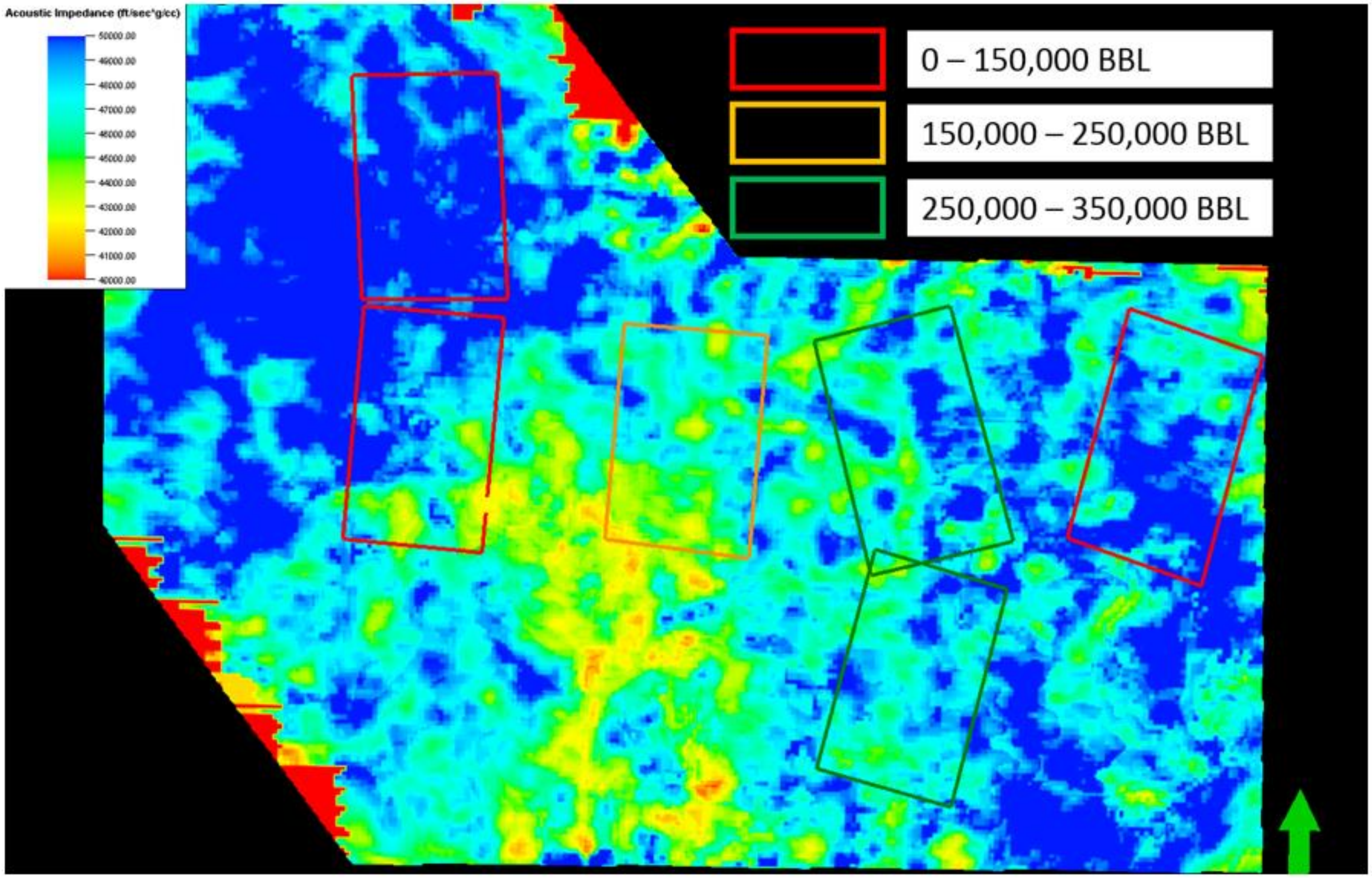

Figure 21. Average acoustic impedance was computed for the entire Mississippi interval. Warmer colors indicate lower acoustic impedance. Boxes were traced around the extent of the hydraulic fracture stimulated volume assuming a 1500 feet fracture half-length and colored based on first year total fluid production (oil and gas). The compilation shows a fair ($R^2 = 0.34$; P value = 0.252) correlation between total fluid production and acoustic impedance.

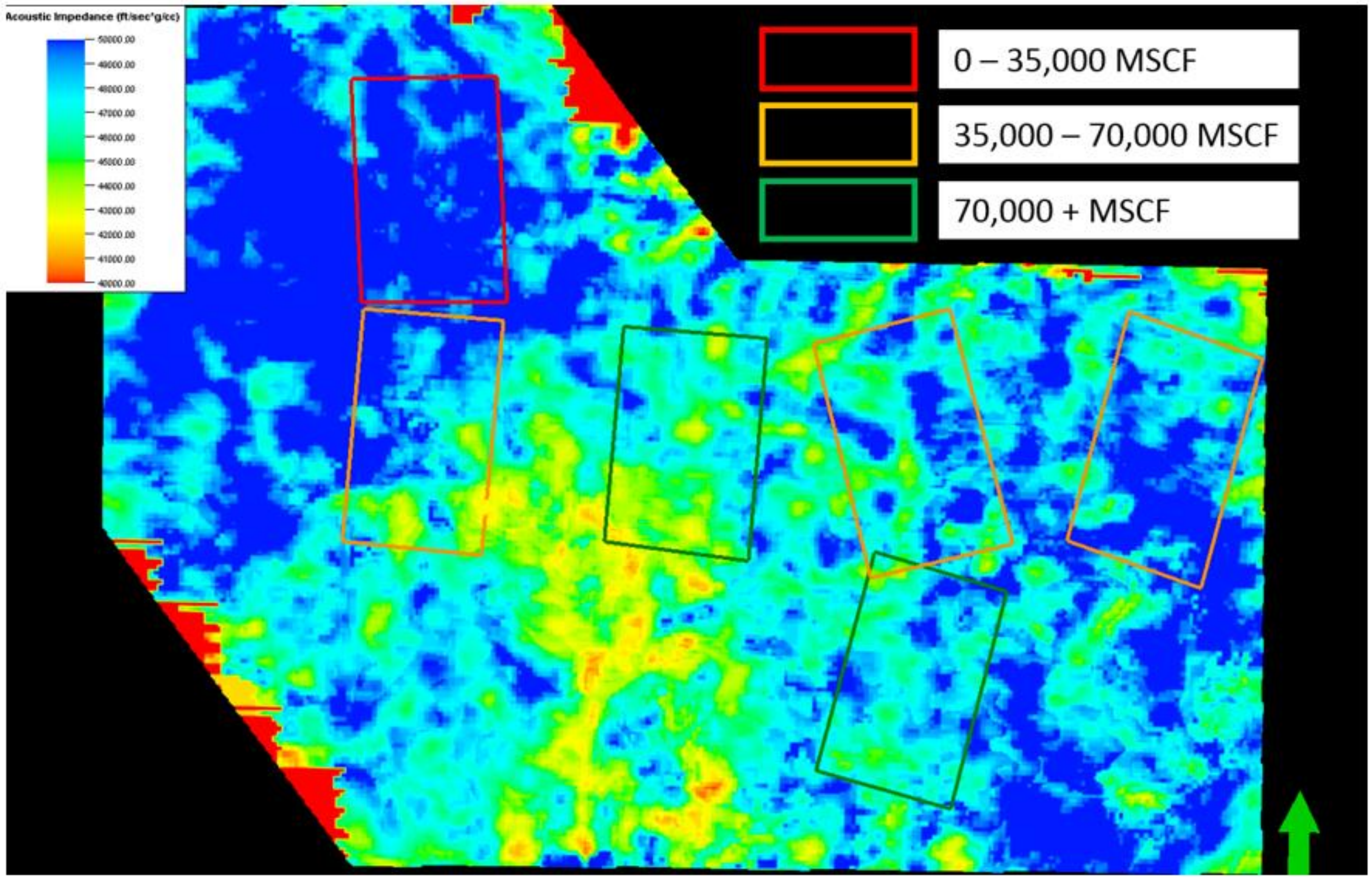

Figure 22. Average acoustic impedance was computed for entire Mississippi interval. Warmer colors indicate lower acoustic impedance. Boxes were traced around the extent of the hydraulic fracture stimulated volume assuming a 1500 feet fracture half-length and colored based on first year gas production. The compilation shows good correlation ($R^2 = 0.68$; P value = 0.0447) between gas production and acoustic impedance.

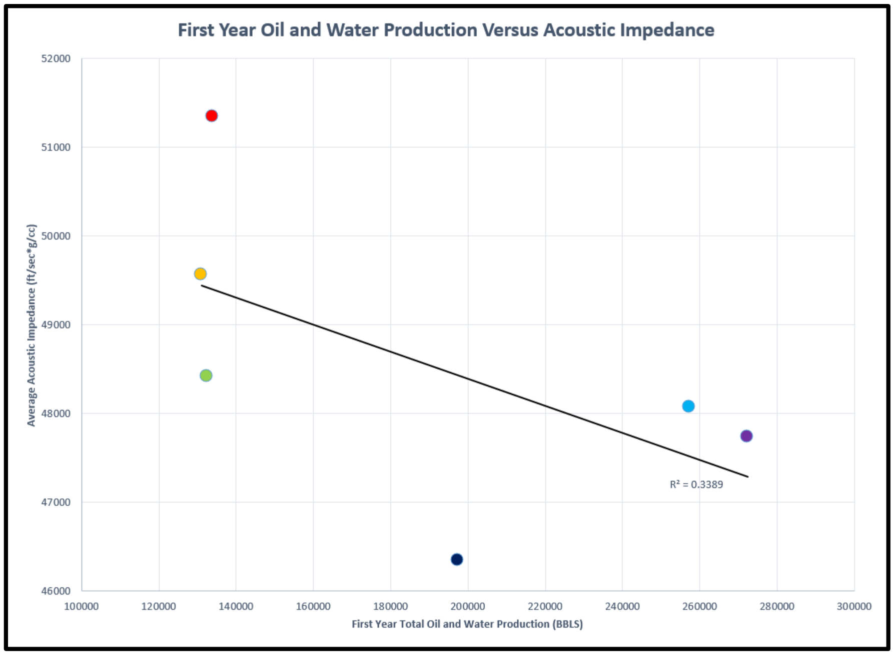

Figure 23. Crossplot of average acoustic impedance, within hydraulic fracture stimulated volume (assuming 1500 feet fracture half length), versus first year total fluid (oil and water) production shows a fair correlation ($R^2 = 0.34$; P value = 0.252). Points are colored by well and are the same in all figures.

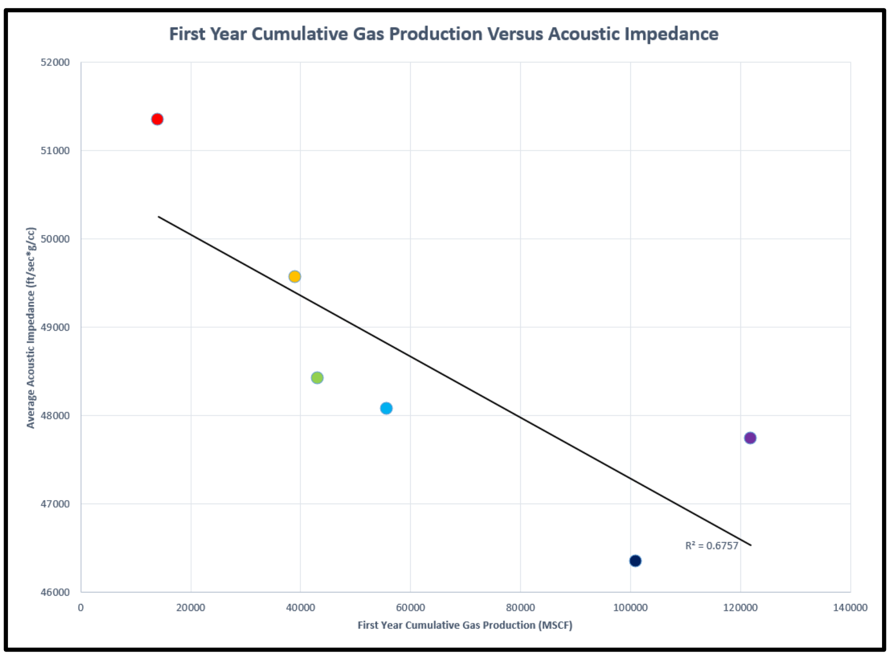

Figure 24. Crossplot of average acoustic impedance, within hydraulic fracture stimulated volume (assuming 1500 feet fracture half length), versus first year gas production shows a good correlation ($R^2 = 0.68$; P value = 0.0447). Points are colored by well and are the same in all figures.

Conclusions

The Mississippian interval located in southern Noble county Oklahoma is composed of a series of stacked cleaning upward clinoforms capped by a higher porosity altered zone historically referred to as “chat”. Analysis of core and seven horizontal image logs show that the brittle upper portion of the clinoforms contain small scale, lithology bound, East-West striking mineralized fractures. In contrast, the ductile lower portion of the clinoforms are less fractured. Total conductive and resistive fracture counts observed from borehole images show no correlation to hydraulically fractured horizontal well productivity. However, the fractures characteristics observed in borehole image logs are only valid for the geomechanical unit the wellbore transects and does not measure fracture geometry away from the wellbore into other geomechanical units. Since the boreholes were landed within a specific reservoir unit, the data do not statistically sample the variability of multiple geomechanical units comprising the Mississippian interval. For this reason, quantifying the mineralized fractures effects on hydraulically fractured horizontal performance was inconclusive.

Structurally related fractures are a function of strain, lithology and layer thickness. Volumetric curvature is a good measure of structural deformation (strain), but does not predict fractures generated from other mechanisms. While not as good an indicator as Gamma Ray at the borehole scale, acoustic impedance is able to differentiate major lithologic units and porosity at the seismic scale. First year total fluid (R^2 = 0.34; P value = 0.252) and gas (R^2 = 0.68; P value = 0.0447) production positively correlate with impedance and were generally higher in areas of low impedance. First year gas production strongly correlated with impedance indicating influence of gas filled porosity.

While volumetric curvature (higher strain) is correlated to fractures in brittle rocks, it is uncorrelated to fractures in ductile rocks. Multiple attributes, be they well-based or seismic-based, are need to characterize fractures in reservoirs comprised of multiple geomechanical units as fractures may be restricted within brittle intervals.

References

Blakey, R., 2015, Paleogeography and geologic evolution of North America; images that tract the ancient landscapes of North America: http://jan.ucc.nau.edu/~rcb7/index.html,(accessed December 1, 2015)

Cahoj, M., and K.J. Marfurt, 2014, Correlating curvature to fault propagation in clay modeled transfer zones: SEG Abstract.

Chopra, S., and K.J. Marfurt, 2010, Integration of coherence and volumetric curvature images: The Leading Edge, **29**, 1092-1107.

Comer, J. B., 1991, Stratigraphic analysis of the Upper Devonian Woodford Formation, Permian Basin, West Texas and Southeastern New Mexico, Bureau of Economic Geology Report of Investigations, no. 201, 20-35.

Dowdell, B.L., 2013, Prestack seismic analysis of a Mississippi Lime resource play in the Midcontinent, U.S.A.: Master's Thesis, The University of Oklahoma, Norman.

Dolton, G.L., and T.M. Finn, 1989, Petroleum geology of the Nemaha Uplift, central Mid-Continent: U.S. Geological Survey, Open-File Report 88-450-D, 30 p.

Gatewood, L.E., 1970, Oklahoma City Field-Anatomy of a Giant, in Halbouty, M.(ed.), Geology of Giant Petroleum Fields: AAPG Memoir **14**, 223-254.

Gay, S.P., 2003, The Nemaha Trend - A System of Compressional Thrust-Fold, Strike-Slip Structural Features In Kansas and Oklahoma: Shale Shaker, July-August 2003, 9-17.

Hart, B. S., and R. Pearson, 2002, 3-D seismic horizon-based approaches to fracture swarm sweet spot definition in tight-gas reservoirs: The Leading Edge, **21**, 28-35.

Harris, P.M., Kenter, J., Playton, T., Andres, M., Jones, G., Levy, M., 2011, Enhancing subsurface reservoir models – An integrated approach using outcrop analogs, modern analogs, and forward stratigraphic models: Search and Discovery Article #50418, AAPG Annual Convention and Exhibition, Houston, TX, April, 1-39.

Jordan, L., and T.L. Rowland, 1959, Mississippian Rocks in Northern Oklahoma: Tulsa Geological Society Digest, **27**, 124-136

Manger, W., 2014, Tripolitic Chert Development in the Mississippian Lime: New Insights from SEM: AAPG Mississippi Lime Forum

Mazzullo, S.J., Wilhite, B.W., Boardman, D.R., 2011, Lithostratigraphic Architecture of the Mississippian Reeds Spring Formation In Southwest Missouri, Northwest Arkansas, and Northeast Oklahoma: Outcrop Analog of Subsurface Petroleum Reservoirs: Shale Shaker, March-April, 254-269.

Northcut, R.A. and J.A. Campbell., 1995, Geologic provinces of Oklahoma: Oklahoma Geological Survey Open-File Report 5-95, 1 sheet, scale 1:750,000, 6-page explanation and bibliography.

Nelson, R.A., 2001, Geologic analysis of naturally fractured reservoirs: Boston, Gulf Professional Pub.

Rector, J., 2011, AAPG Mississippi Lime Forum

Roberts, A., 2001, Curvature attributes and their application to 3D interpreted horizons: First Break, **19**, 85-99.

Rogers, S. M., 2001, Deposition and diagenesis of Mississippian chat reservoirs, northcentral Oklahoma, AAPG Bulletin, **85**, 115-130.

Sigismondi, M. E., and J.C. Soldo, 2003, Curvature attributes and seismic interpretation: Case studies from Argentina basins: The Leading Edge, **22**,1122-1126.

Stearns, D.W., and M. Friedman, 1972, Reservoirs in Fractured Rock, in Stratigraphic Oil and Gas Fields, AAPG. Memoir **16**, 82-106.

Staples, E., 2011, Subsurface and experimental analysis of fractures and curvature: M.S. Thesis, U. of Oklahoma.

Turnini, A.M., 2015, Stratigraphic and Structural Controls on Mississippian Limestone and Tripolitic Chert Reservoir Distribution Using Seismic-Constrained Reservoir Characterization and Modeling, Northern Oklahoma: Master’s Thesis, The University of Oklahoma, Norman.

Trumbo, D.B., 2014, A Production Calibrated Reservoir Characterization of the Mississippi Lime in a Mature Field Utilizing Reprocessed Legacy 3D Seismic Data, Kay County, Oklahoma: Master’s Thesis, The University of Oklahoma, Norman.

White, H.G., 2013, Fracturing of Mississippi Lime, Oklahoma: Experimental, Seismic attributes and Image Logs Analyses: Master’s Thesis, The University of Oklahoma, Norman.

Young, E.M., 2010, Controls on Reservoir Character in Carbonate-Chert Strata, Mississippian (Osagean-Meramecian), Southeast Kansas: Master’s Thesis, The University of Kansas, Lawrence.

Appendix A: Borehole Image Interpretation

The following figures are examples of interpreted fractures from the 7 interpreted horizontal wells. Fractures were classified based on their relative resistivity to the matrix as either resistive or conductive. Figures A1 and A2 are of resistive fractures. Figures A3 and A4 are of conductive fractures. Figures A5 and A6 are of reactivated or reopened resistive/mineralized fractures.

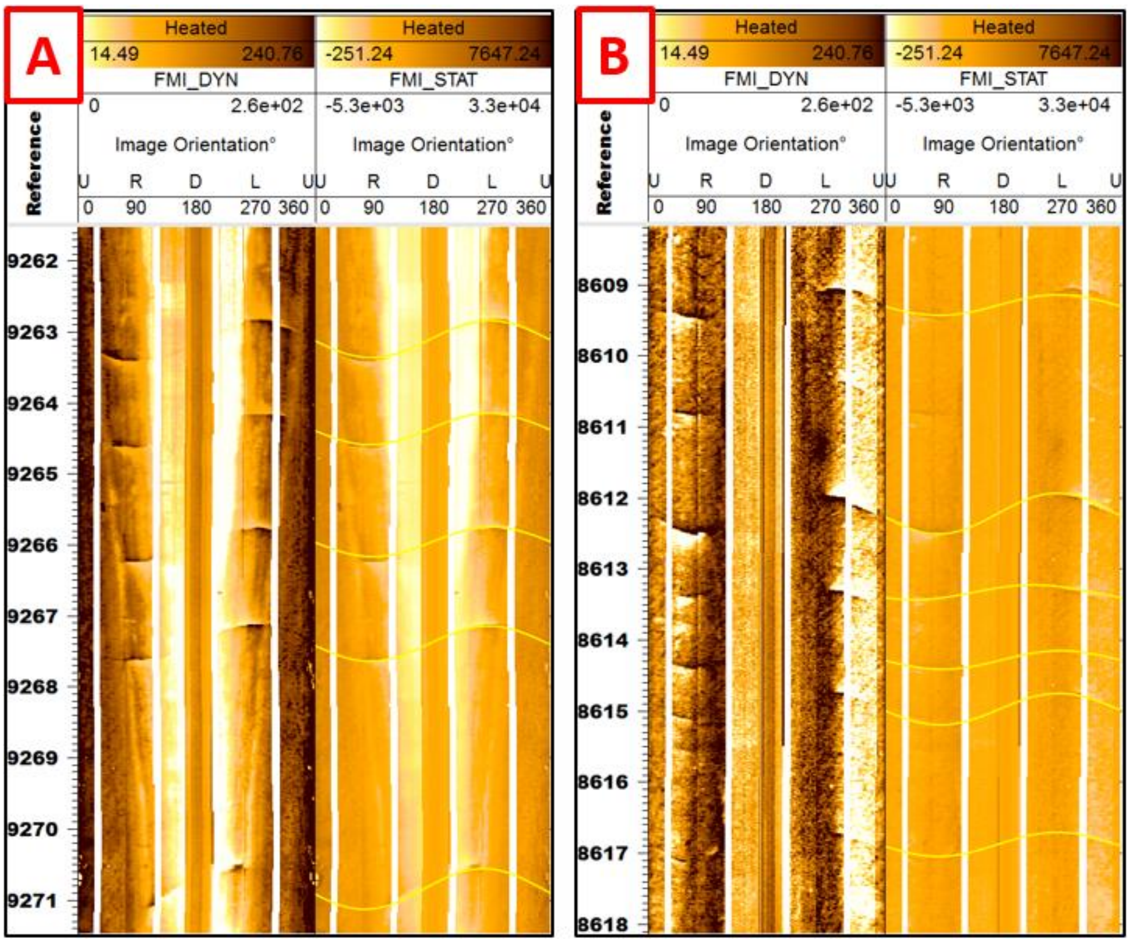

Figure A1. Examples of resistive fractures observed. The fractures are classified as resistive based on their relative resistivity to that of the matrix. Resistive fractures are often distinguished by a distinct resistive "halo" that is an artifact of data acquisition.

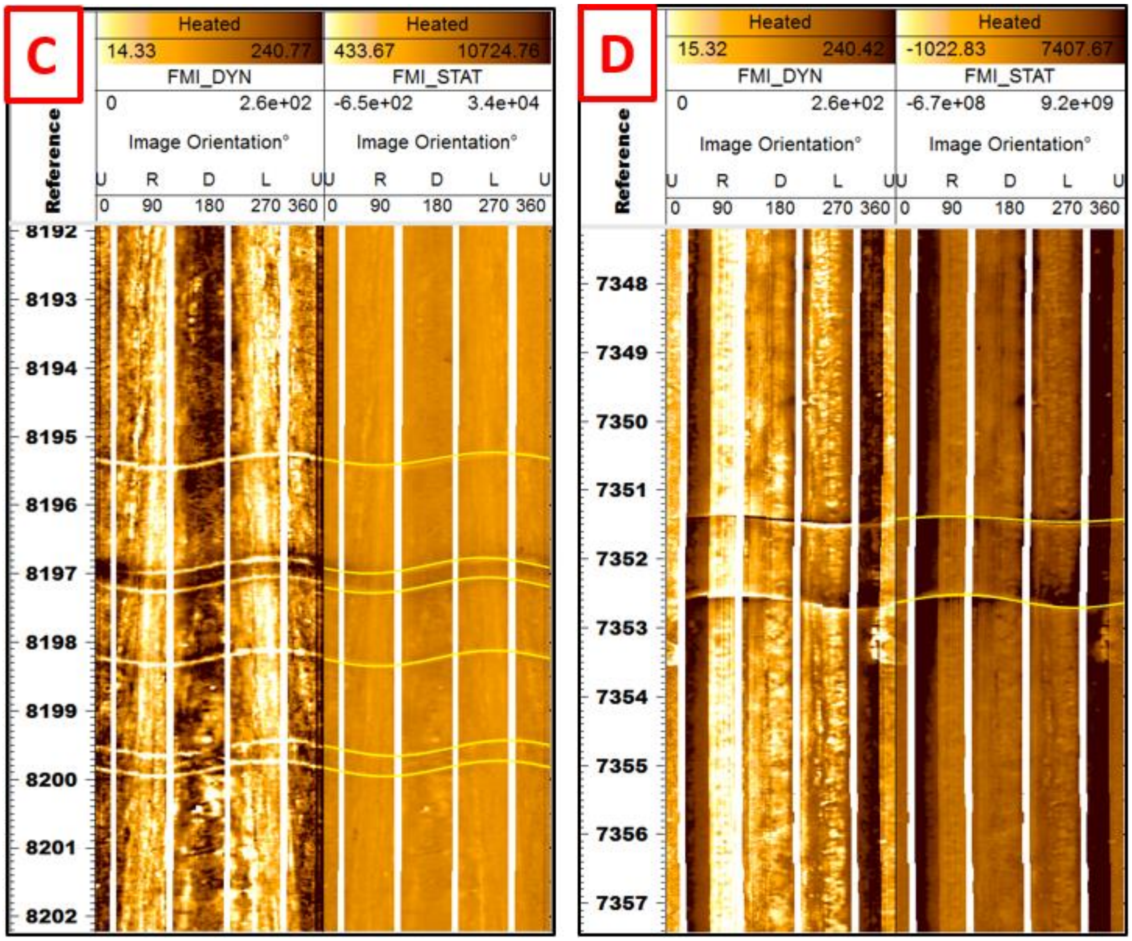

Figure A2. Examples of resistive fractures observed. The fractures are classified as resistive based on their relative resistivity to that of the matrix. Resistive fractures are often distinguished by a distinct resistive "halo" that is an artifact of data acquisition. Note that in image C the halo effect is not evident.

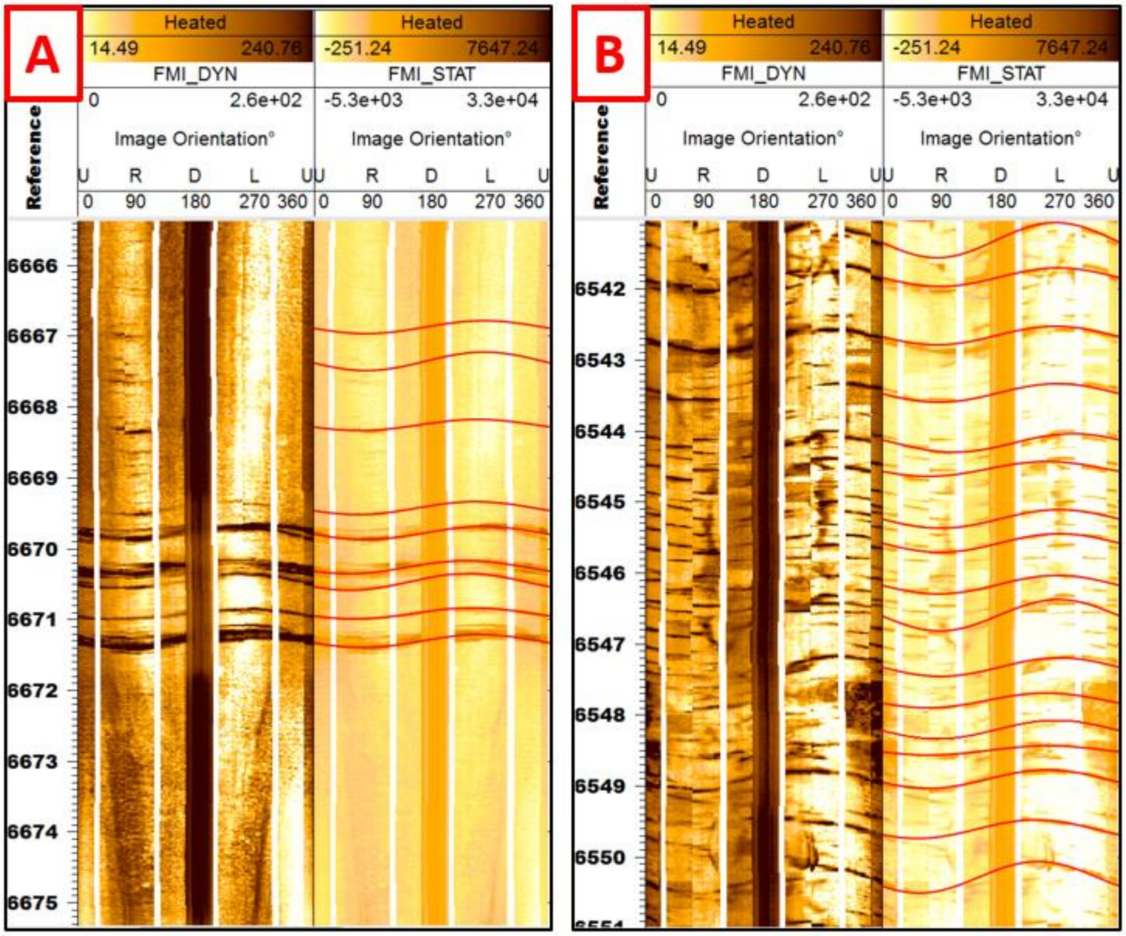

Figure A3. Examples of conductive fractures observed. Conductive fractures are classified based on their relative resistivity to that of the matrix. Open fractures allow conductive mud invasion into the fracture plane. The fracture appears conductive relative to the surrounding matrix by the borehole image tool. Note that image B has a processing artifact called pad-flap mismatch causing the fractures to appear discontinuous.

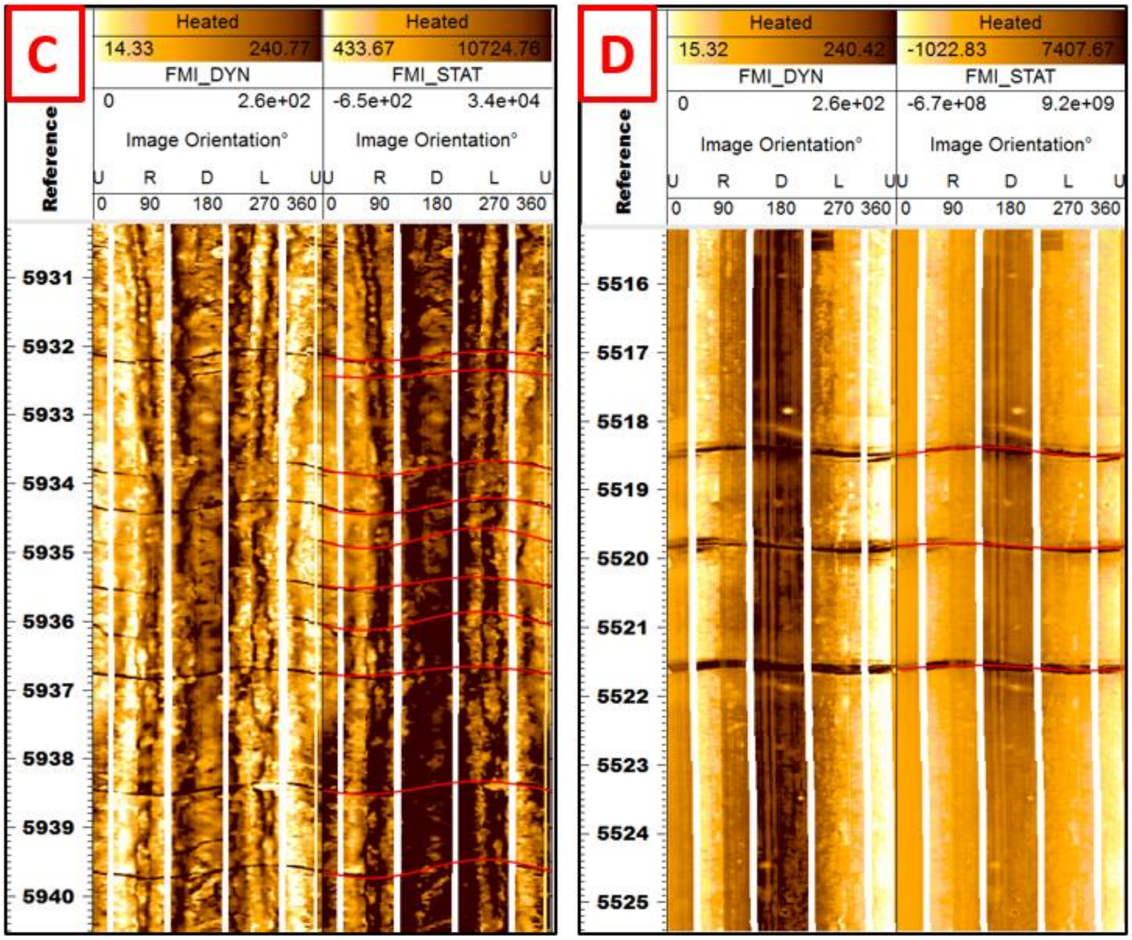

Figure A4. Examples of conductive fractures observed. Conductive fractures are classified based on their relative resistivity to that of the matrix. Open fractures allow conductive mud invasion into the fracture plane. The fracture appears conductive relative to the surrounding matrix by the borehole image tool.

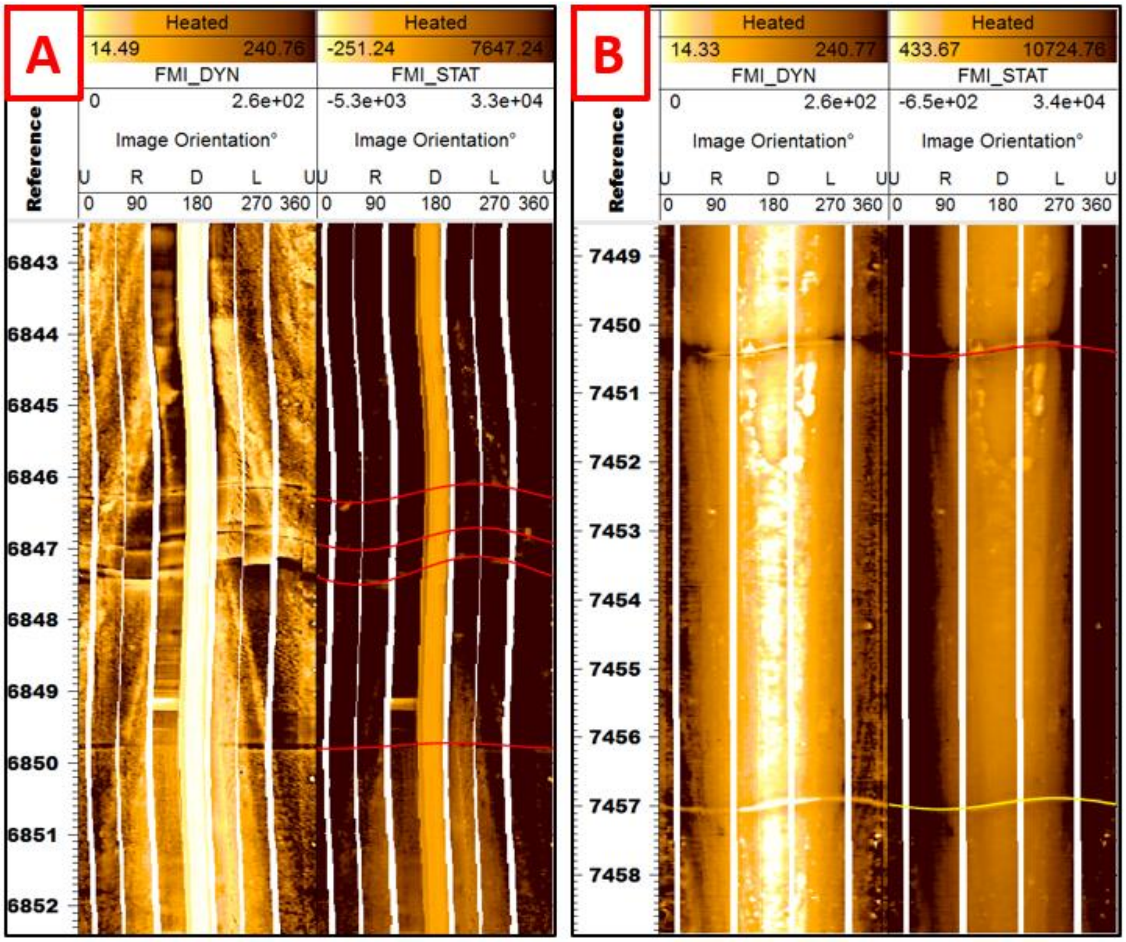

Figure A5. Examples of mineralized fractures that are partially conductive. Mud invasion into the fracture plane could occur in fractures that are not completely mineralized. Completely mineralized fractures could also be reactivated by drilling and fluid stresses allowing conductive fluid entry.

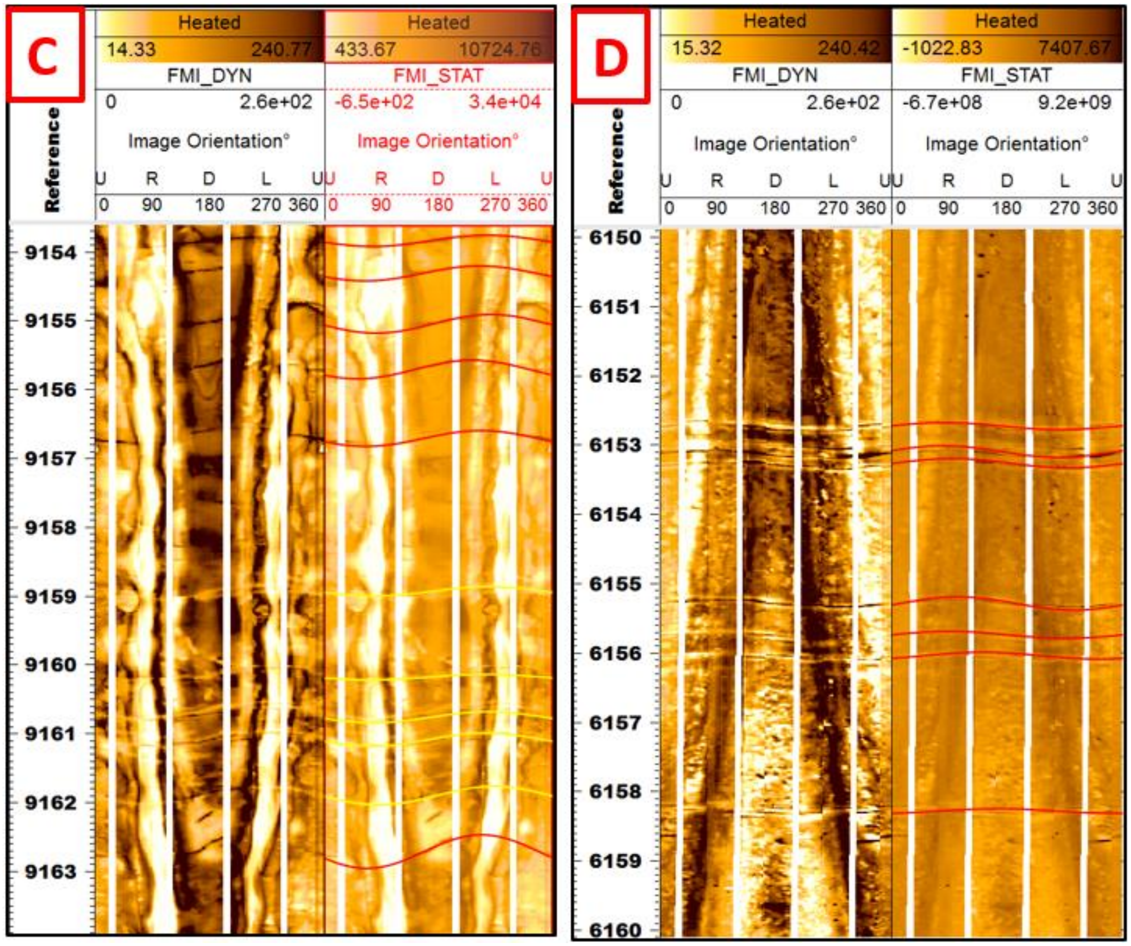

Figure A6. Examples of mineralized fractures that are partially conductive. Mud invasion into the fracture plane could occur in fractures that are not completely mineralized. Completely mineralized fractures could also be reactivated by drilling and fluid stresses allowing conductive fluid entry.

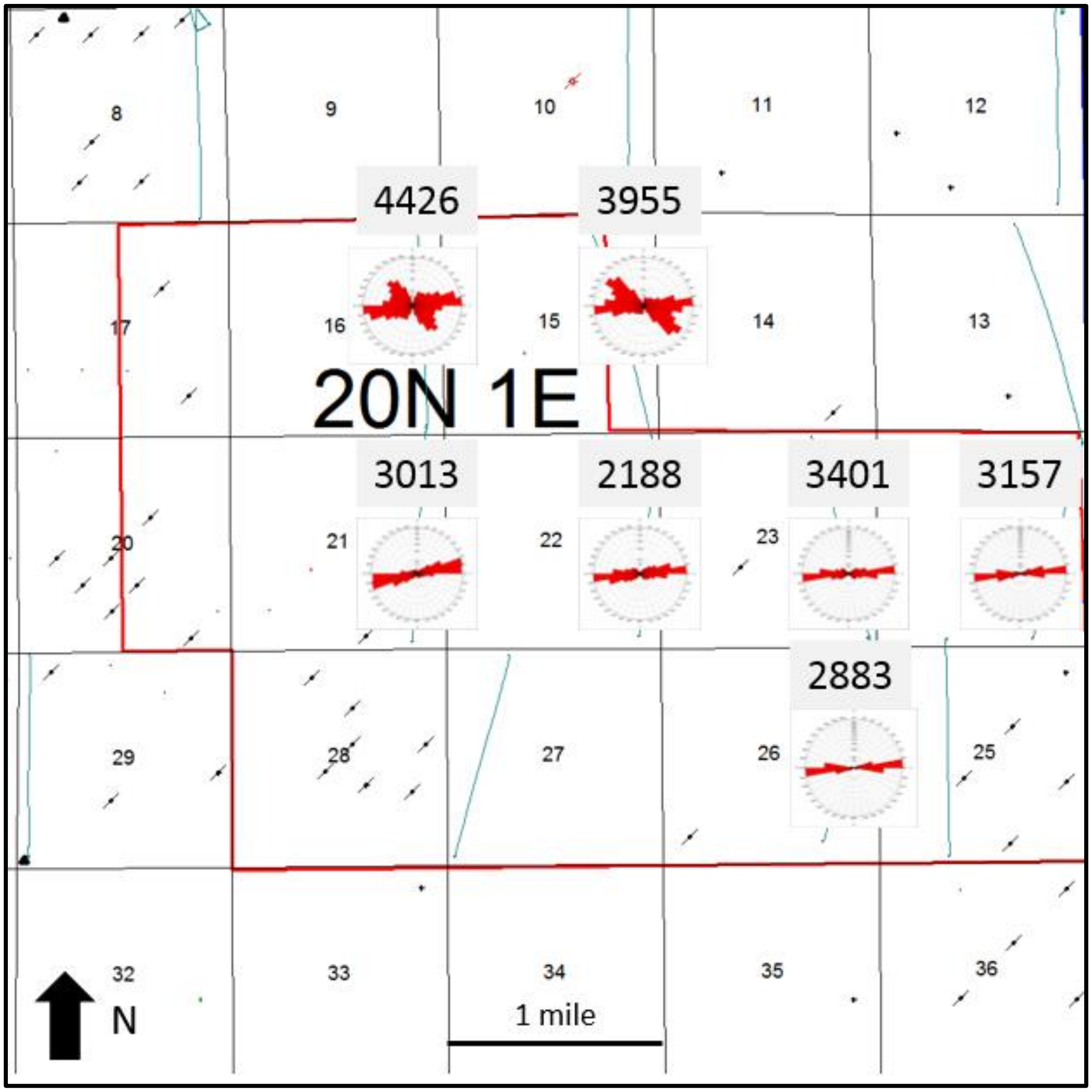

Figure A7. Strike rosettes of the interpreted conductive fractures are plotted on top of the respective wells. The gross number of conductive fractures for each well are plotted above each respective rosette. The dominant strike orientation of the conductive fracture sets is East-West. Two wells also have a bimodal fracture set striking Northeast-Southwest.

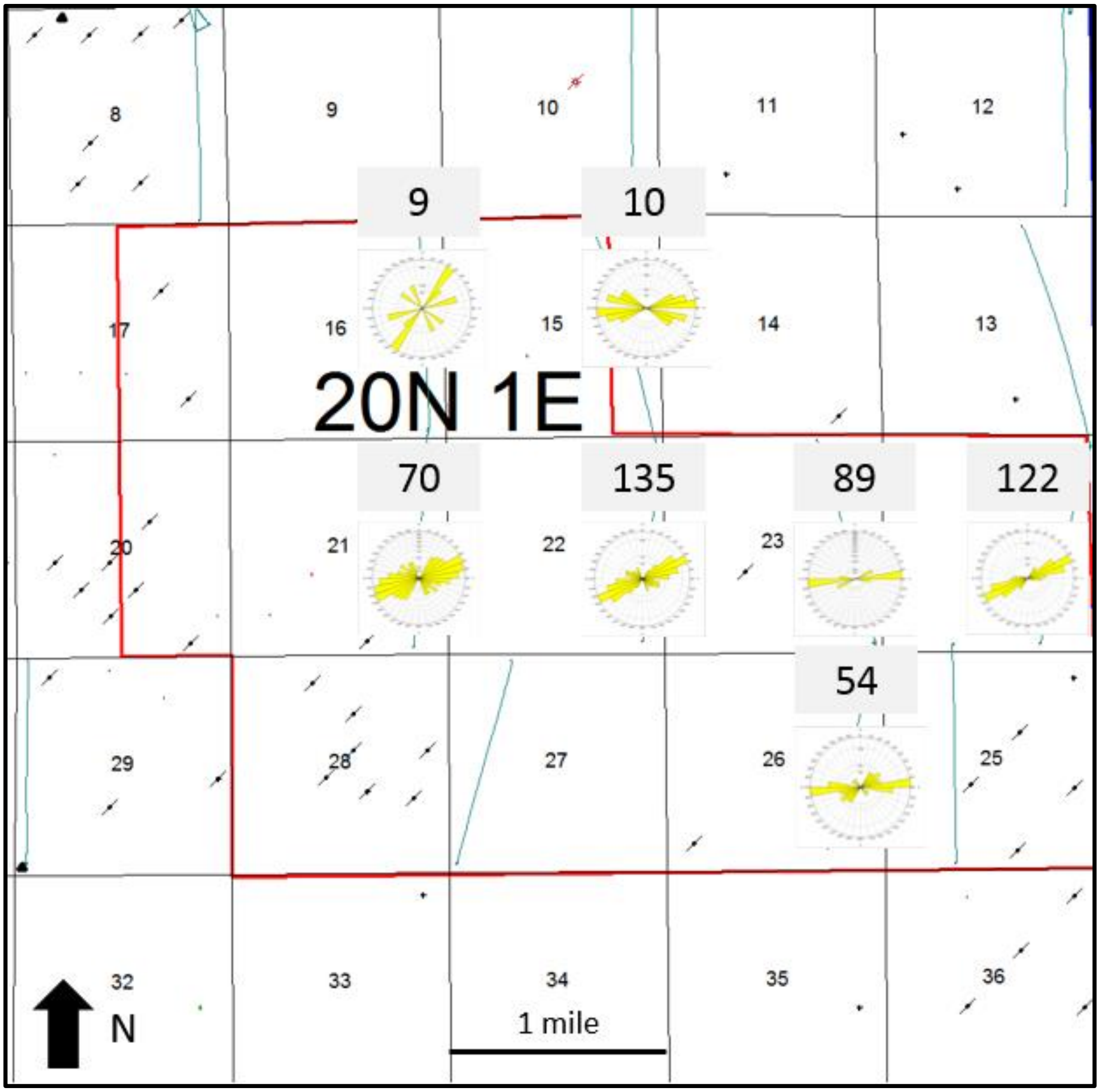

Figure A8. Strike rosettes of the interpreted resistive fractures are plotted on top of the respective wells. The gross number of resistive fractures for each well are plotted above each respective rosette. The dominant strike orientation of the resistive fracture sets is East-West with some scatter. Two wells have slightly shifted orientations striking East Northeast – West Southwest. Scatter in one well is due to limited number of observed fractures.

Appendix B: Core Analysis

Figure B1. Core photos from the Gulf Oil Flora 1 showing two distinct lithologies observed. A chert bed can be seen in photo A from 4692.5-4693.2 ft. The massive lime mudstone lithology can be seen throughout the entire core in photo B.

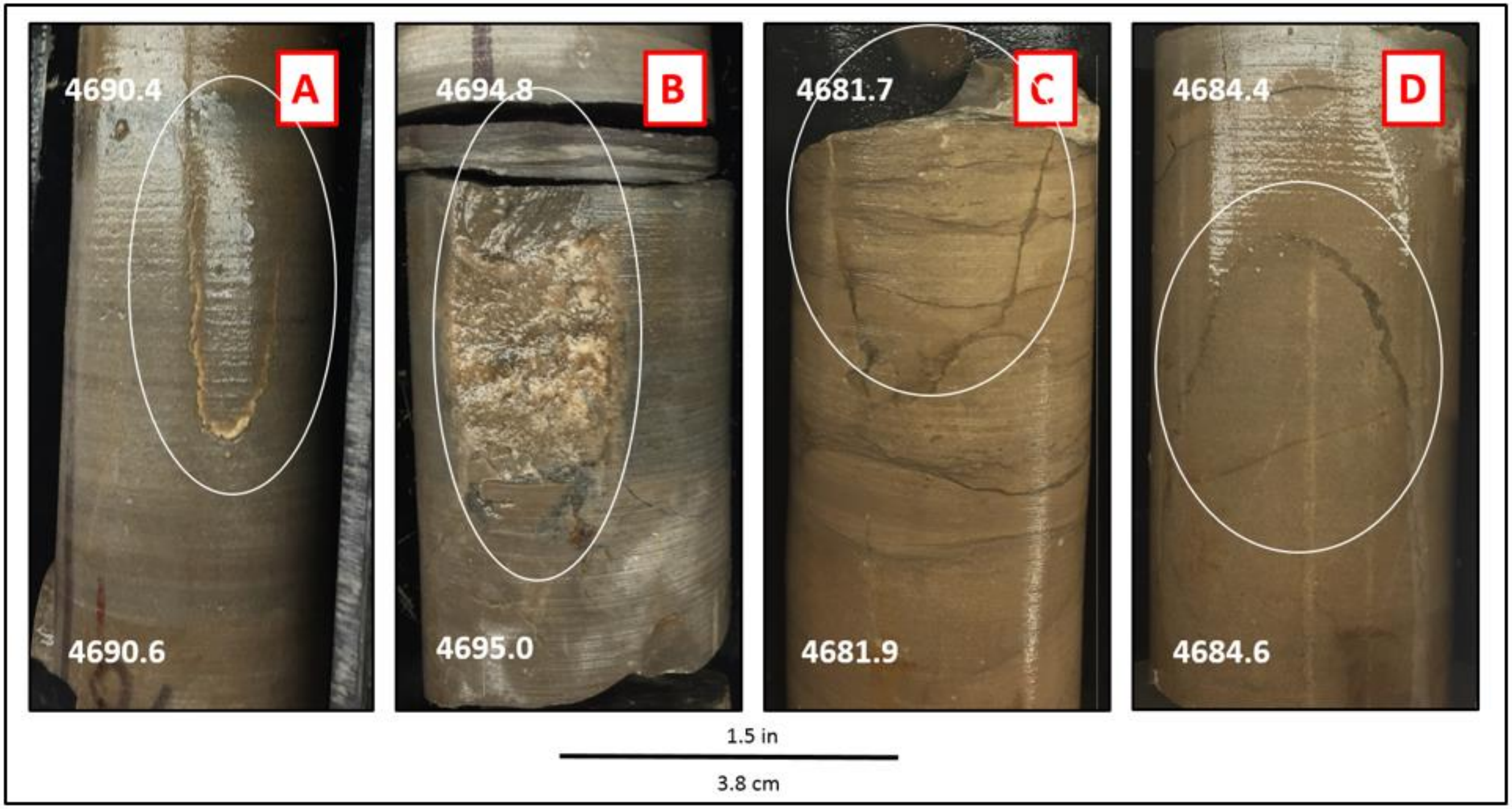

Figure B2. Core photos from the Gulf Oil Flora 1 showing mineralized fractures. All fractures shown above terminate within the core. Complete mineralization is seen in photos C and D. In photo B, the core was chipped along the fracture plane revealing the mineral precipitate.

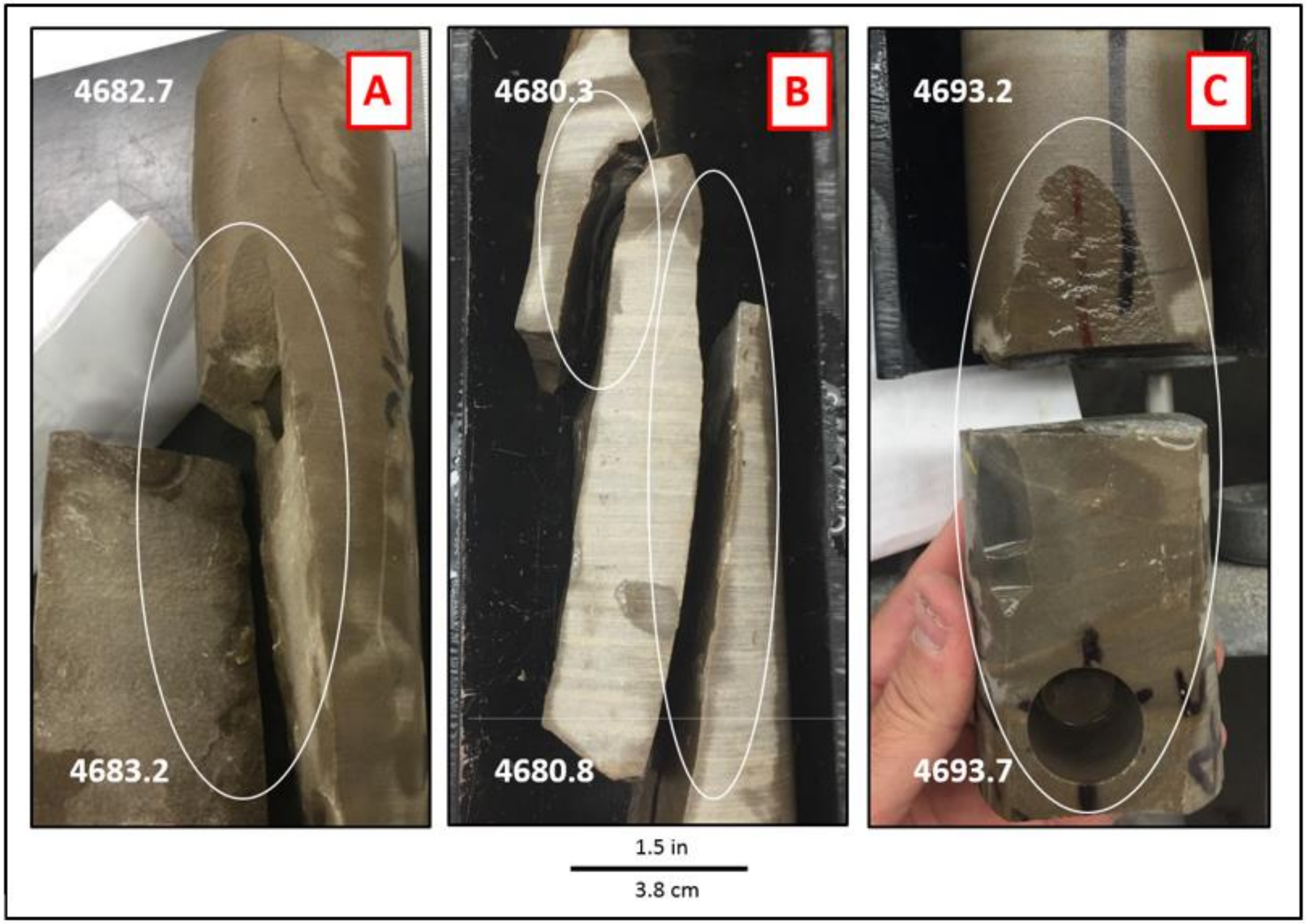

Figure B3. Core photos from the Gulf Oil Flora 1 showing possible open natural fractures. Diagnosing the origin as natural or induced from coring and retrieval was not possible.

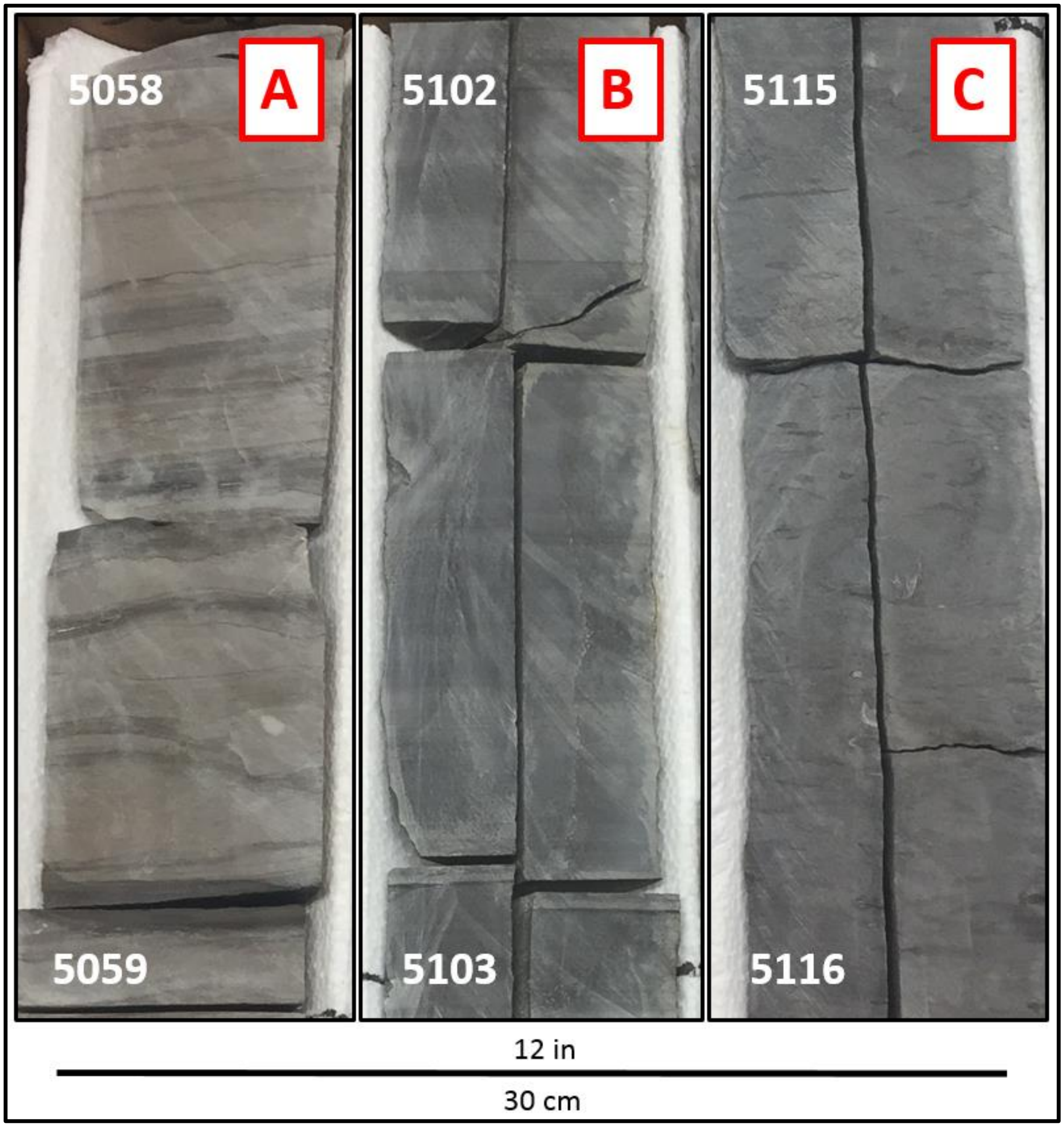

Figure B4. Core photos from the Double Eagle Tubbs No. 3 showing three distinct lithologies. Wavy bedded lime mudstone (A), planar bedded lime mudstone (B), and bioturbated lime mudstone (C) can be observed above.

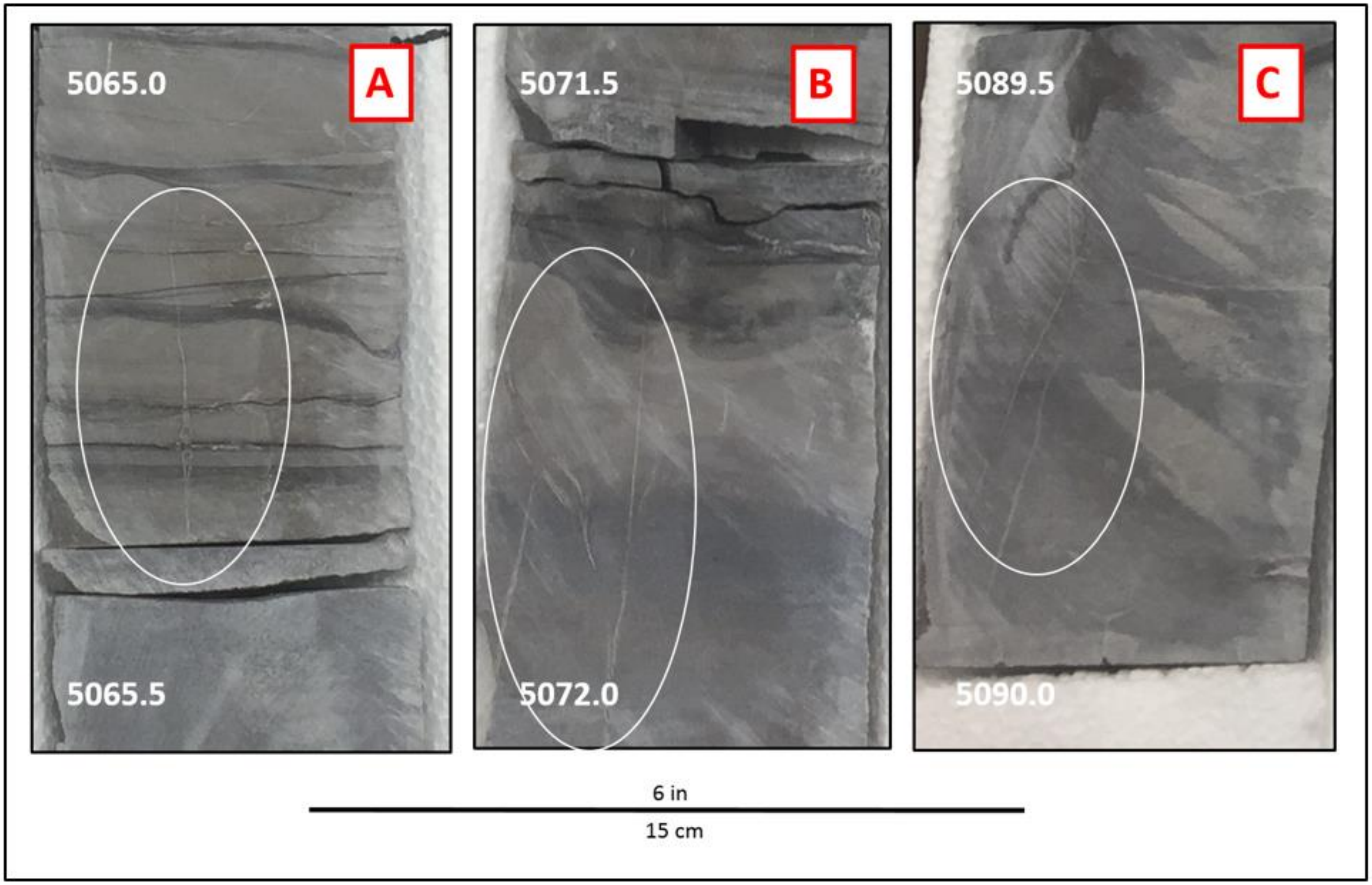

Figure B5. Core photos from the Double Eagle Tubbs No. 3 showing mineralized fractures. Fracture termination can be observed in all fractures shown above.

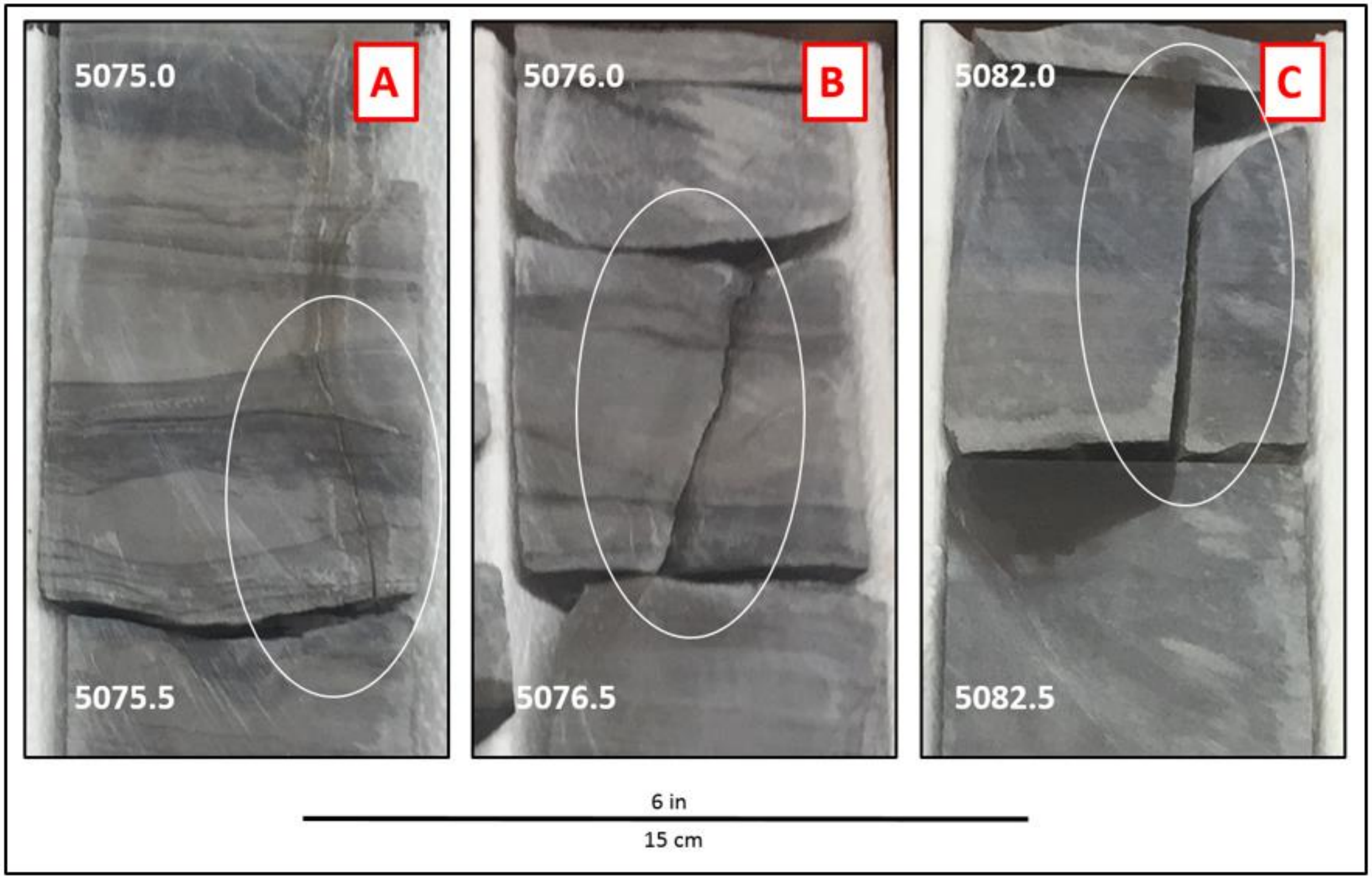

Figure B6. Core photos from the Double Eagle Tubbs No. 3 showing possible open fractures. The fracture in photo A appears to be partially mineralized. Diagnosing the origin of the open fractures observed above as natural or induced from coring and retrieval was not possible.

Appendix C: Well Log Correlation

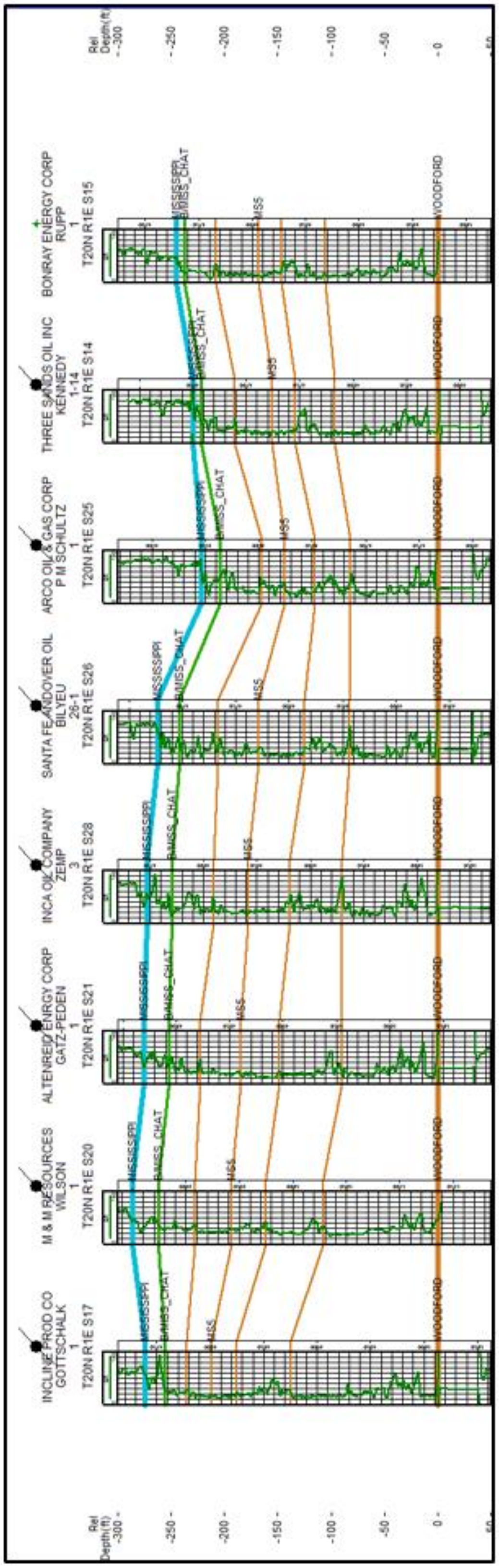

Figure C1. Cross section of all vertical well logs available within study area. Internal Mississippian gamma ray markers were correlated in all wells.

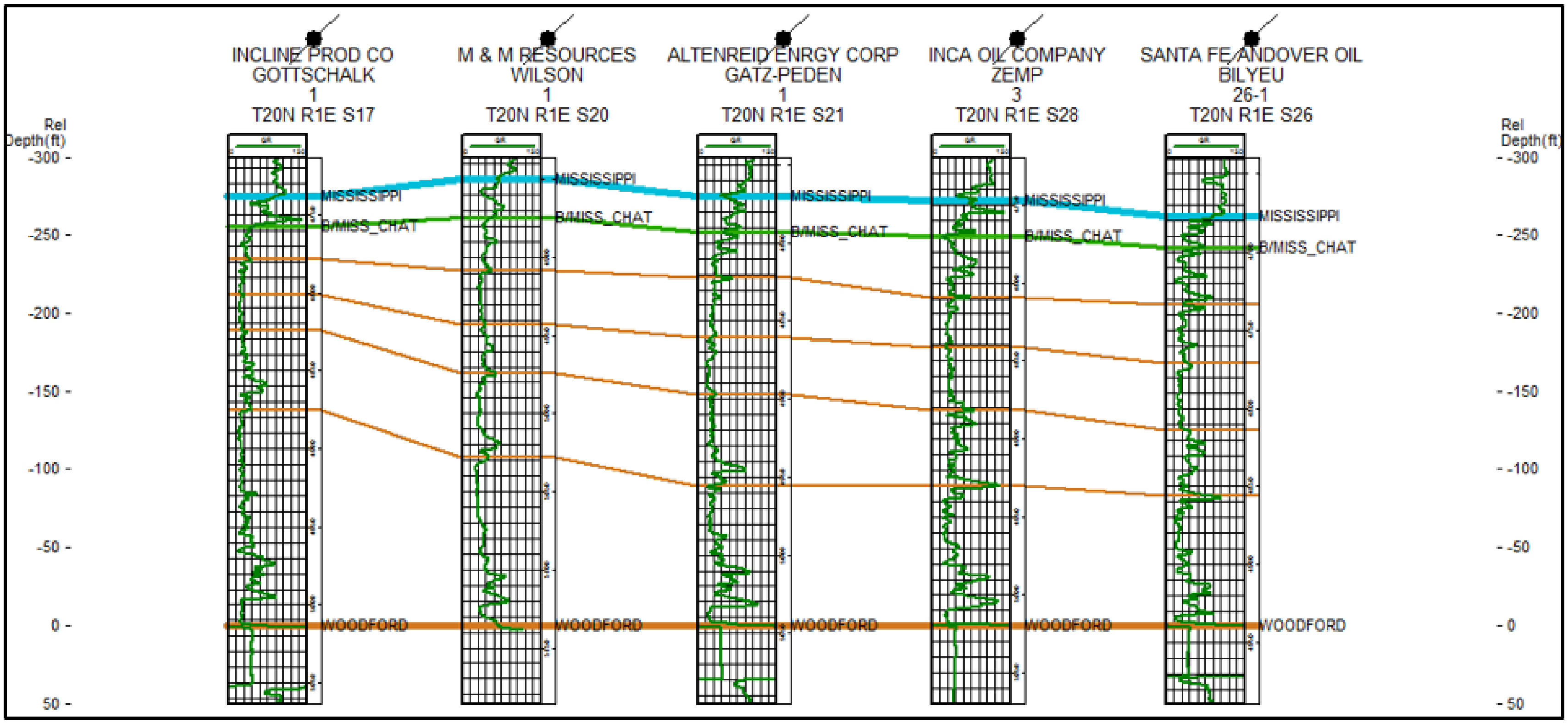

Figure C2. Cross section along clinoform dip illustrating nature of internal Mississippian gamma ray marker beds and clinoform structure.

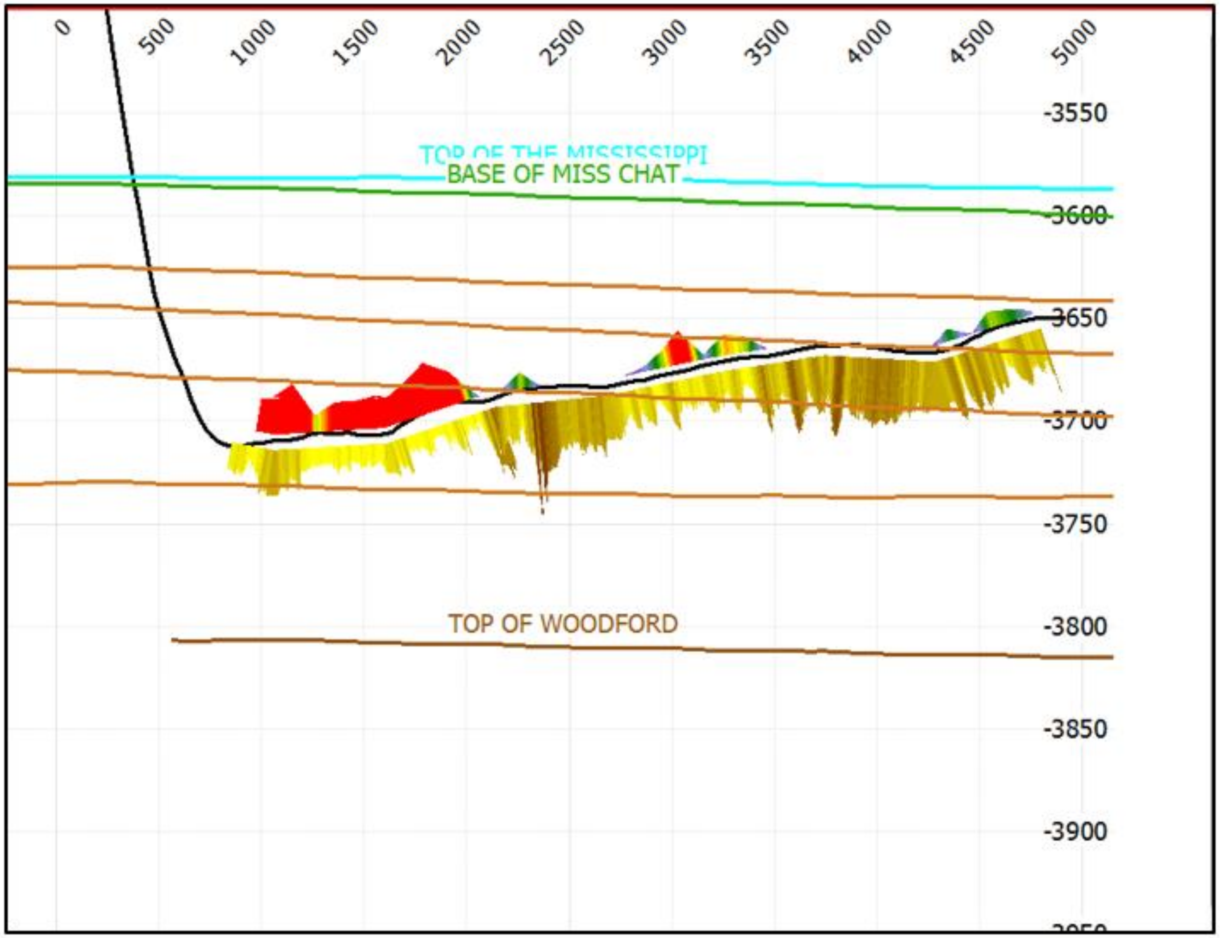

Figure C3. Well section showing horizontal well traversing through high gamma ray marker beds. Fracture density is plotted along the upper portion of the wellbore with red indicating more than 5 and blue indicating 0 fractures per foot. Gamma Ray is displayed along the bottom of the wellbore with yellow indicating 10 GAPI or less and brown indicating 80 or more. Fracture density is high in low Gamma Ray rock and vice versa.

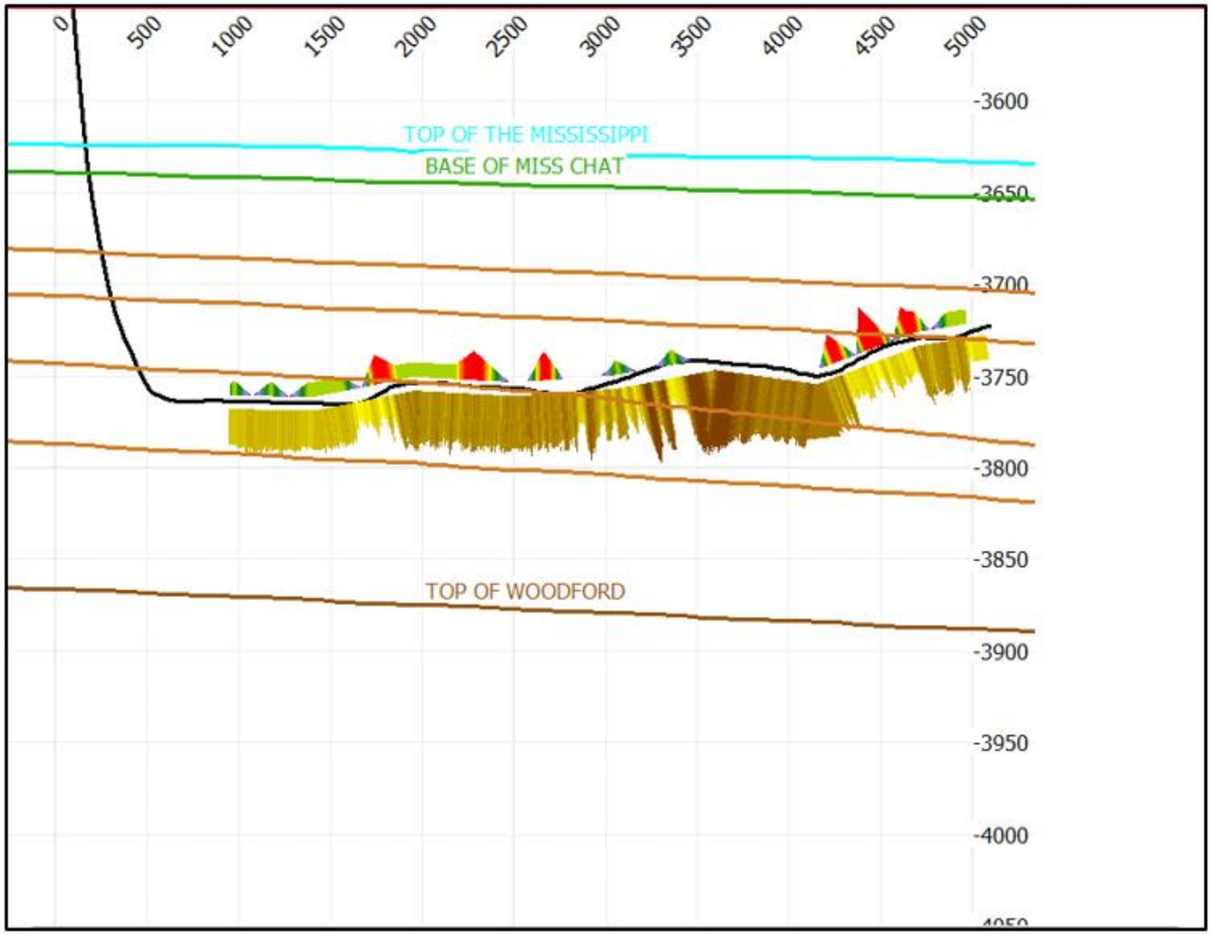

Figure C4. Well section showing horizontal well traversing through high gamma ray marker beds. Fracture density is plotted along the upper portion of the wellbore with red indicating more than 5 and blue indicating 0 fractures per foot. Gamma Ray is displayed along the bottom of the wellbore with yellow indicating 10 GAPI or less and brown indicating 80 or more. Thickness of gamma ray beds and limited vertical well control affects correlation. Fracture density is greater in low Gamma Ray beds.

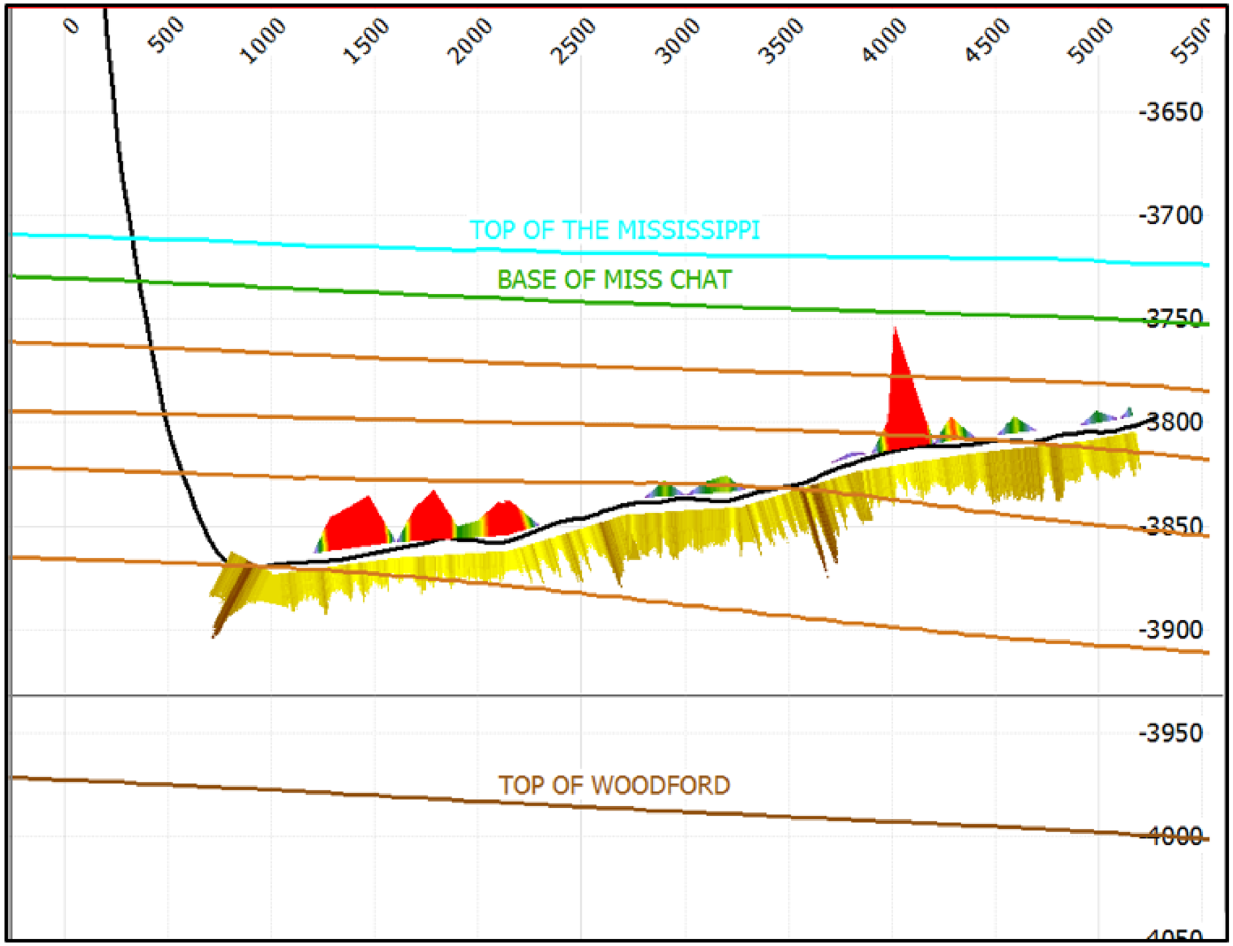

Figure C5. Well section showing horizontal well traversing through high gamma ray marker beds. Fracture density is plotted along the upper portion of the wellbore with red indicating more than 5 and blue indicating 0 fractures per foot. Gamma Ray is displayed along the bottom of the wellbore with yellow indicating 10 GAPI or less and brown indicating 80 or more. Fracture density is high in low Gamma Ray rock and vice versa.

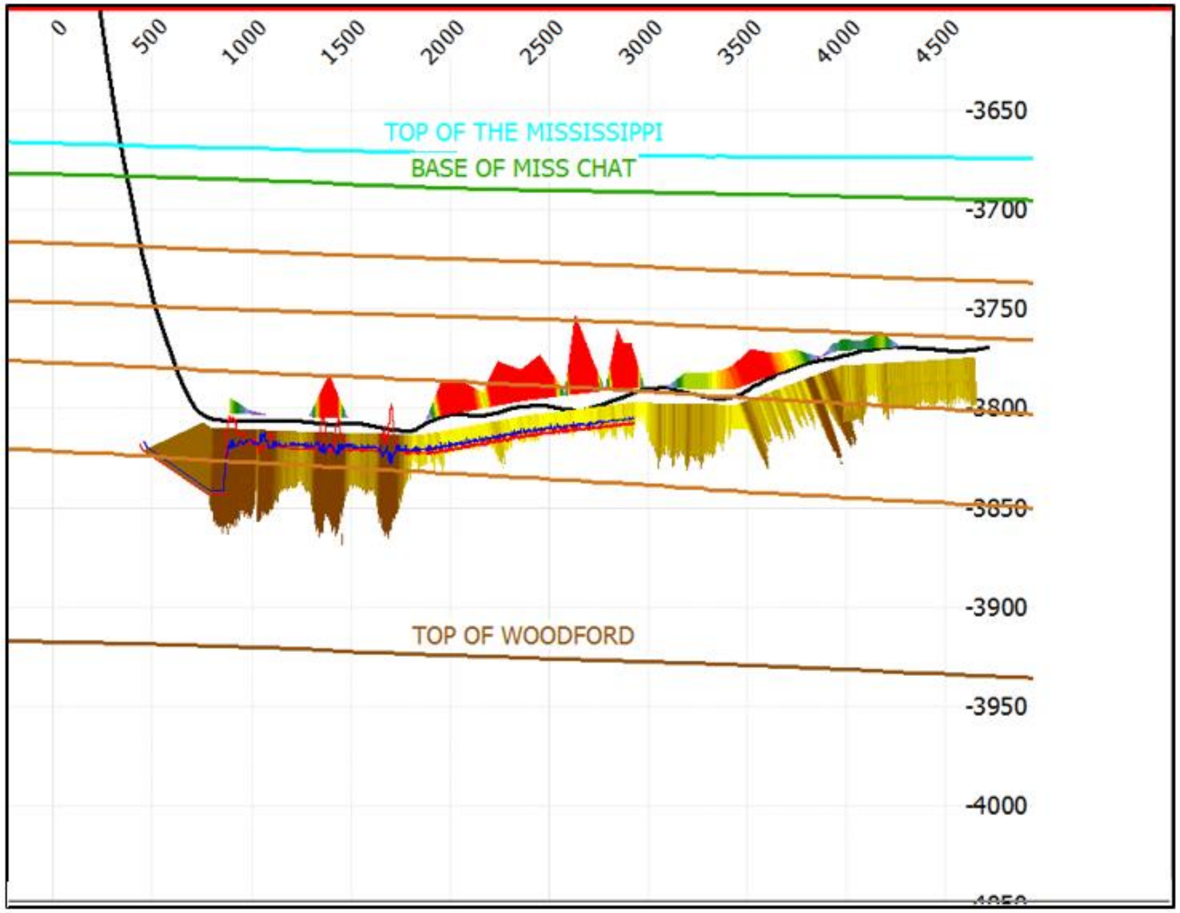

Figure C6. Well section showing horizontal well traversing through high gamma ray marker beds. Fracture density is plotted along the upper portion of the wellbore with red indicating more than 5 and blue indicating 0 fractures per foot. Gamma Ray is displayed along the bottom of the wellbore with yellow indicating 10 GAPI or less and brown indicating 80 or more. Fracture density is high in low Gamma Ray rock and vice versa. Dual axis calipers are also plotted along the bottom of the well path. Gamma Ray spikes high in oval sections hole suggesting shale accumulation in washout.

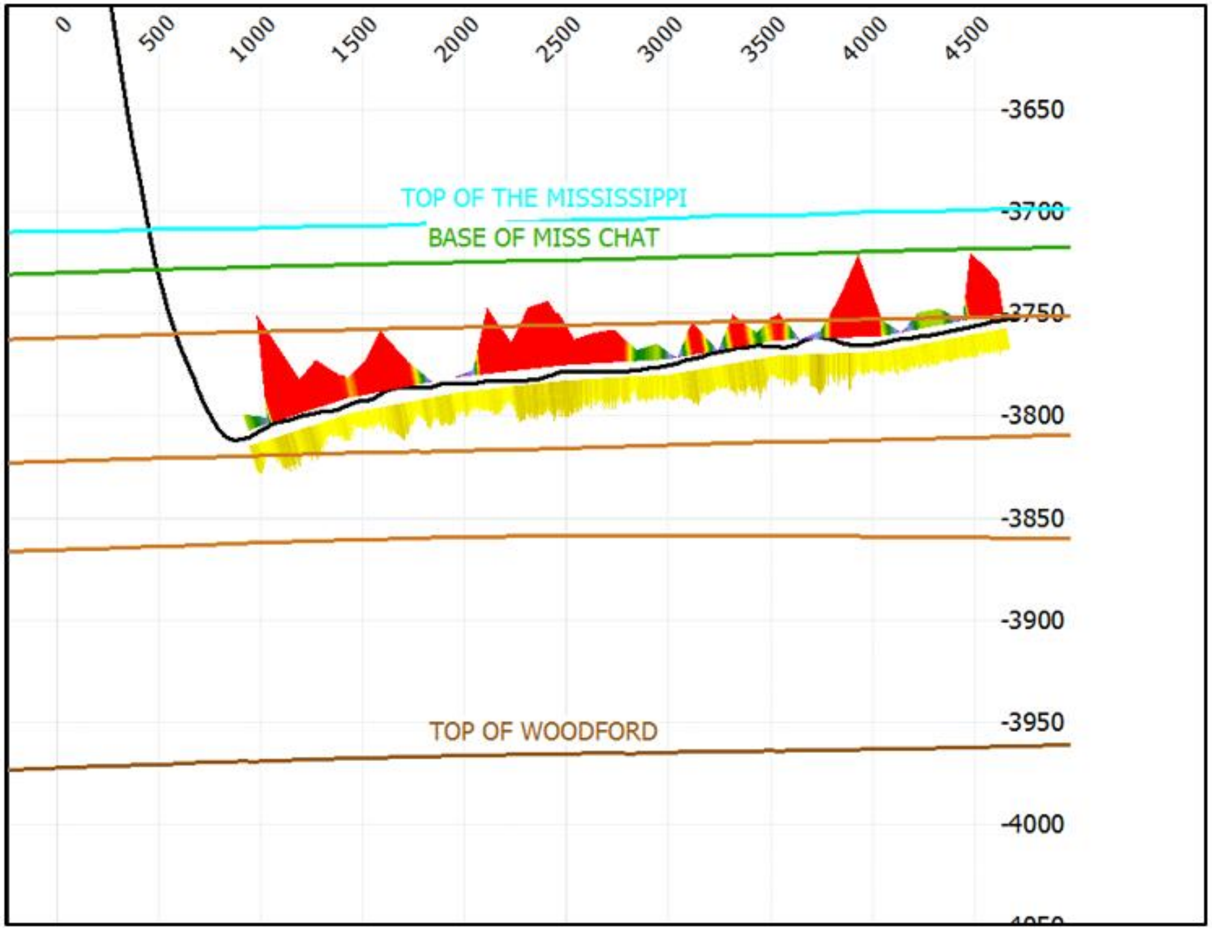

Figure C7. Well section showing horizontal well traversing between high gamma ray marker beds. Fracture density is plotted along the upper portion of the wellbore with red indicating more than 5 and blue indicating 0 fractures per foot. Gamma Ray is displayed along the bottom of the wellbore with yellow indicating 10 GAPI or less and brown indicating 80 or more. Fracture density is high in low Gamma Ray rock.

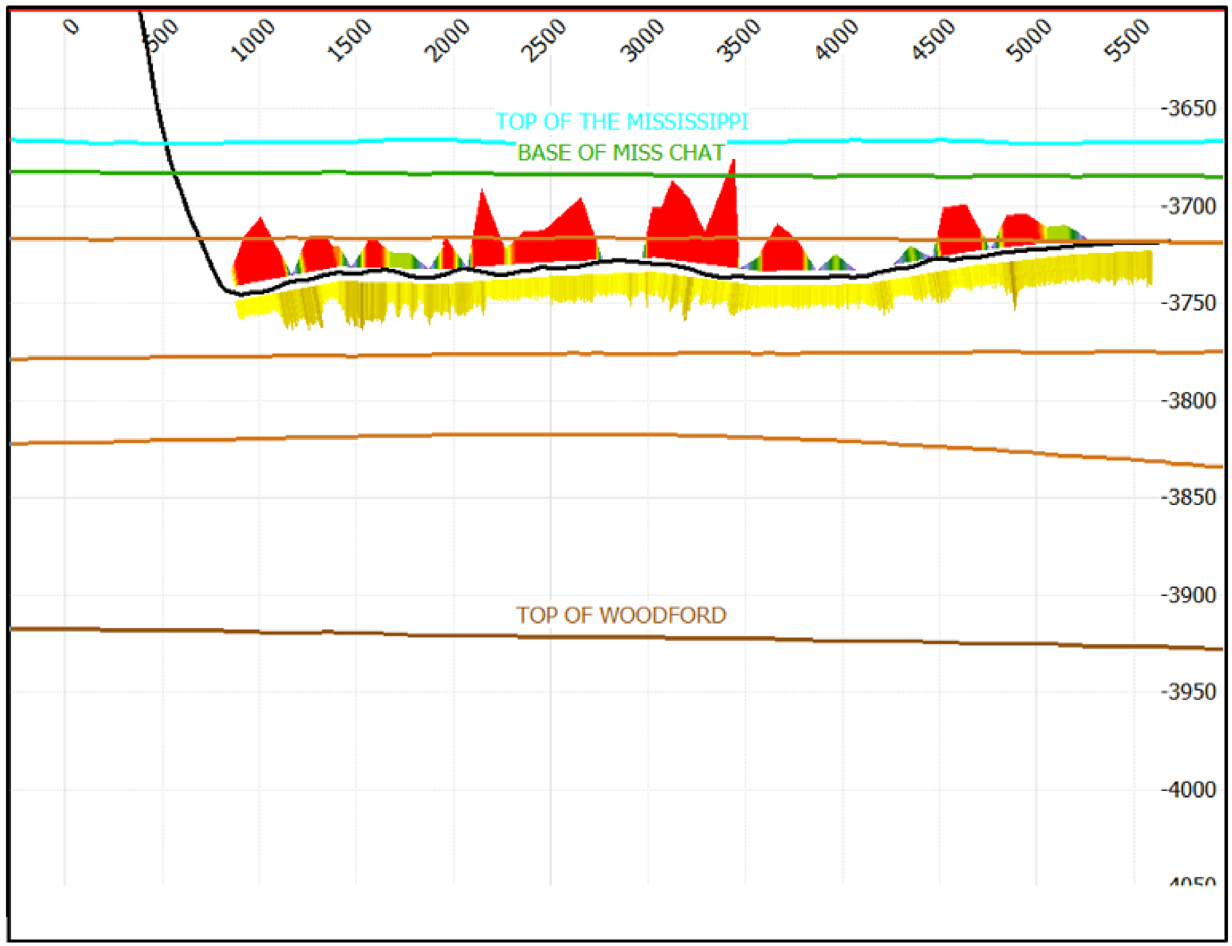

Figure C8. Well section showing horizontal well traversing between high gamma ray marker beds. Fracture density is plotted along the upper portion of the wellbore with red indicating more than 5 and blue indicating 0 fractures per foot. Gamma Ray is displayed along the bottom of the wellbore with yellow indicating 10 GAPI or less and brown indicating 80 or more. Fracture density is high in low Gamma Ray rock.

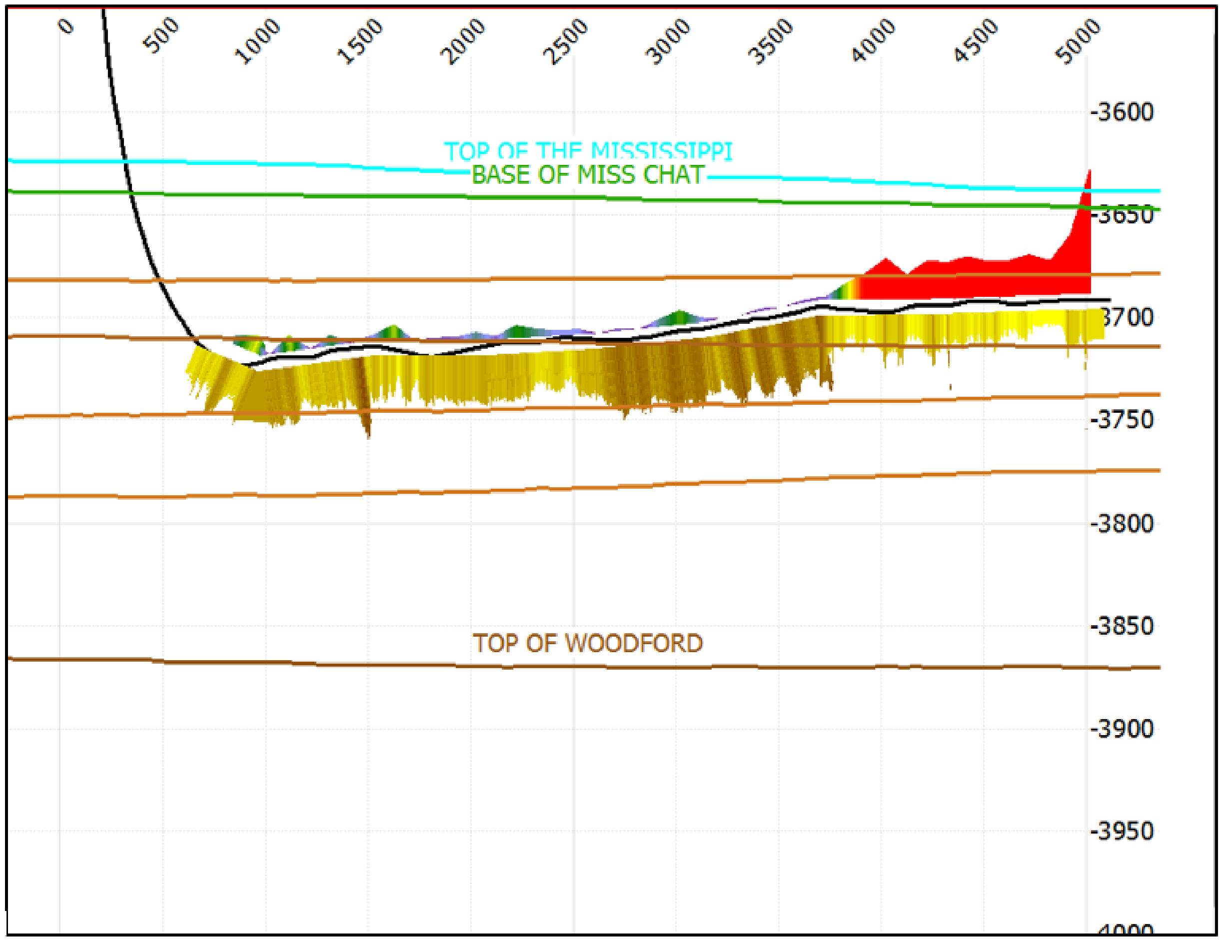

Figure C9. Well section showing horizontal well traversing through high gamma ray marker beds. Fracture density is plotted along the upper portion of the wellbore with red indicating more than 5 and blue indicating 0 fractures per foot. Gamma Ray is displayed along the bottom of the wellbore with yellow indicating 10 GAPI or less and brown indicating 80 or more. Fracture density is high in low Gamma Ray rock and vice versa.

Appendix D: Seismic Data

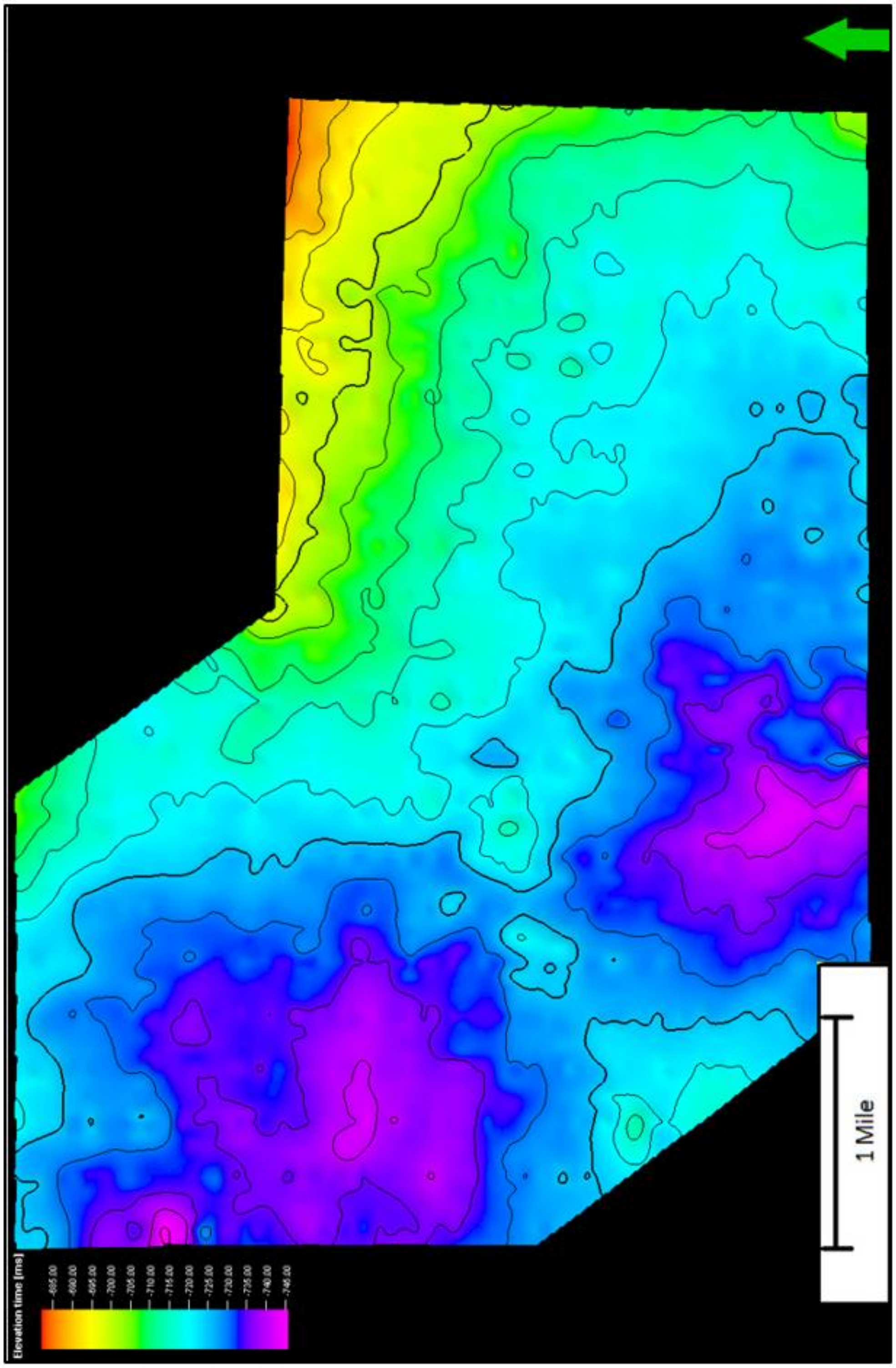

Figure D1. Time structure map of the top of the Mississippian illustrates westerly dip. Warm colors indicate structural highs while cool colors indicate lows.

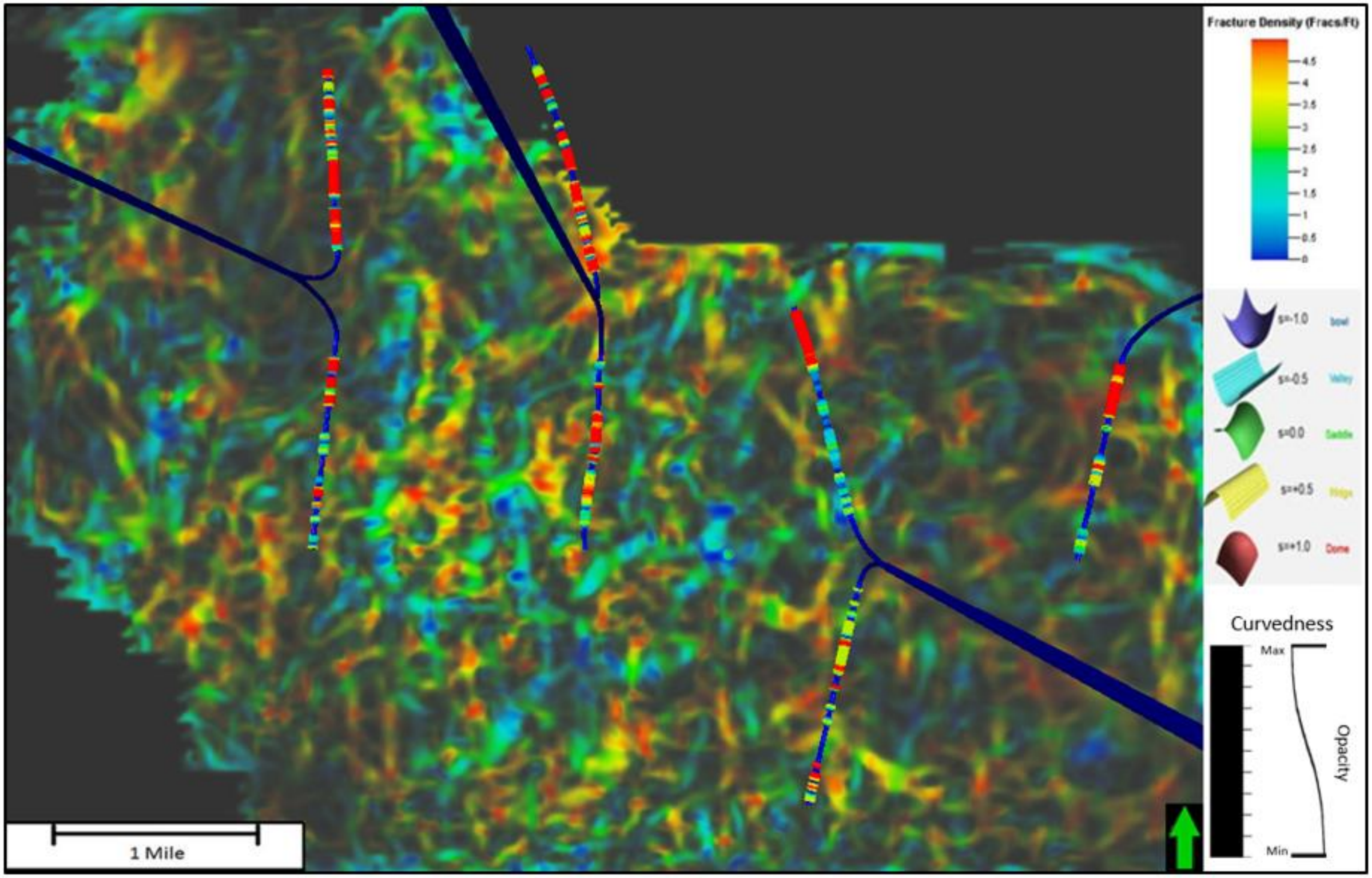

Figure D2. Shape index time slice co-rendered with Curvedness through Mississippian illustrates internal structure. Fracture data displayed as a 3D pipe along the wellbores with red indicating more than five and blue indicating zero fractures per foot.

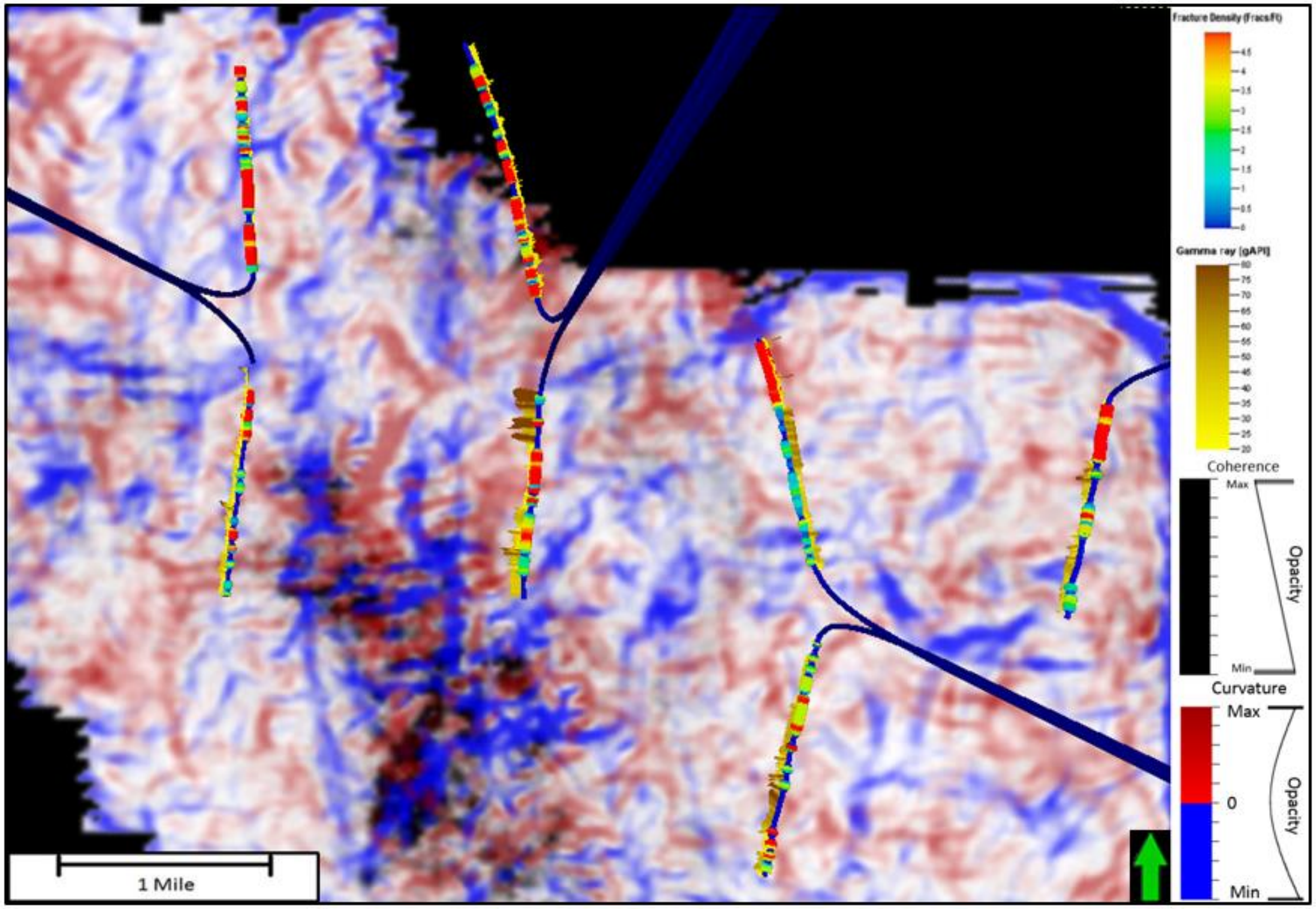

Figure D3. Most-positive and most-negative curvature time slice through Mississippian illustrates internal structure. Fracture data displayed as a 3D pipe along the wellbores with red indicating more than five and blue indicating zero fractures per foot. Gamma Ray is displayed as a 2D log along the wellbores with yellow indicating 10 GAPI or less and brown indicating 80 or more.